The Heart of China revisited: II Early Paleozoic (ultra)high-pressure and (ultra)high-temperature metamorphic Qinling orogenic collage

Thomas Bader,[1,2] Leander Franz,[1] Lothar Ratschbacher,[3] Christian de Capitani,[1] A. Alexander G. Webb,[4] Zhao Yang,[3] Jörg A. Pfänder,[3] Mandy Hofmann,[5] and Ulf Linnemann[5]

Received 3 September 2012; revised 6 June 2013; accepted 10 June 2013; published 6 August 2013.

[1] Orogens with multiple (ultra)high-pressure ((U)HP) and (ultra)high-temperature ((U)HT) metamorphic events provide a complex but telling record of oceanic and continental interaction. The Early Paleozoic history of the "Heart of China," the Qinling orogenic collage, offers snapshots of at least three (U)HP and two (U)HT metamorphic events. The preservation of remnants of both oceanic and continental domains together with a ≥110 Myr record of magmatism allows the reconstruction of the processes that resulted in this disparate metamorphism. Herein, we first illuminate the pressure-temperature-time (P-T-t) evolution of the Early Paleozoic (U)HP and (U)HT events by refining the petrographic descriptions and P-T estimates, assess published, and employ new U/Th-Pb zircon, monazite, and titanite, and ^{40}Ar-^{39}Ar phengite geochronology to date the magmatic and metamorphic events. Then we explore how the metamorphic and magmatic events are related tectonically and how they elucidate the affinities among the various complexes in the Qinling orogenic collage. We argue that a Meso-Neoproterozoic crustal fragment—the Qinling complex—localized subduction-accretion events that involved subduction, oceanic-arc formation, and back-arc spreading along its northern margin, and mtantle-wedge exhumation and spreading-ridge subduction along its southern margin.

Citation: Bader, T., L. Franz, L. Ratschbacher, C. de Capitani, A. A. G. Webb, Z. Yang, J. A. Pfänder, M. Hofmann, and U. Linnemann (2013), The Heart of China revisited: II Early Paleozoic (ultra)high-pressure and (ultra)high-temperature metamorphic Qinling orogenic collage, *Tectonics*, *32*, 922–947, doi:10.1002/tect.20056.

1. Introduction

[2] Stretching E-W more than 2000 km between the North China craton (NCC) and the South China craton (SCC), the Qilian-Qinling-Tongbai-Dabie-Sulu (herein Qinling-Tongbai) orogen constitutes the geographic, geologic, and cultural "Heart of China" (Figure 1) [e.g., *Zhang et al*., 2001]. The Qinling-Tongbai evolution comprised subduction-accretion-collision events in the Neoproterozoic [e.g., *Wang et al*., 2003], Cambrian [e.g., *Yang et al*., 2003], Carboniferous [e.g., *Sun et al*., 2002], and Triassic [e.g., *Okay et al*., 1993]. The study of this orogen has yielded insights into (ultra) high-pressure ((U)HP) and (ultra) high-temperature ((U)HT) metamorphism and tectonics [e.g., *Hacker et al*., 2004; *Liu et al*., 2011; *Cheng et al*., 2012], and the assembly and break-up of the core of the supercontinent Rodinia [e.g., *Li et al*., 2008a; *Bader et al*., 2013]. A decade ago, we [*Ratschbacher et al*., 2003] combined new and published data into a tectonic model of the Qinling-Tongbai orogen. Numerous new data have appeared since. In this series of papers, we assess the literature accessible to us and combine it with our own new petrologic-geochronologic-structural data. The subject herein is the Early Paleozoic (~550–360 Ma) evolution of the Qin Mountains (Qinling) and the Tongbai Mountains (Tongbai Shan) with a focus on the Qinling complex and its relationships to the various rock units (complexes) of the Qinling-Tongbai orogenic collage (i.e., the NCC, Kuanping, Erlangping, Danfeng, Songshugou, and SCC subblocks; Figures 1 and 2).

[3] The principal questions this paper addresses are as follows: (1) What pressure-temperature-time (P-T-t) evolution do the Early Paleozoic (U)HP and (U)HT events in the Qinling-Tongbai orogen involve? We refine petrographic descriptions and P-T estimates of the metamorphic rocks, and employ published and new U/Th-Pb zircon, monazite, and titanite, and ^{40}Ar-^{39}Ar phengite geochronology to highlight the magmatic and metamorphic events. (2) How

Additional supporting information may be found in the online version of this article.

[1]Mineralogisch-Petrographisches Institut, Universität Basel, Basel, Switzerland.
[2]Key Laboratory of Orogenic Belts and Crustal Evolution, MOE, School of Earth and Space Sciences, Peking University, Beijing, China.
[3]Geologie, Technische Universität Bergakademie Freiberg, Freiberg, Germany.
[4]Geology and Geophysics, Louisiana State University, Baton Rouge, Louisiana, USA.
[5]Geochronologie, Senckenberg Naturhistorische Sammlungen, Dresden, Germany.

Corresponding author: L. Ratschbacher, Geologie, Technische Universität Bergakademie Freiberg, 09599 Freiberg, Germany. (lothar@geo.tu-freiberg.de)

0278-7407/13/10.1002/tect.20056

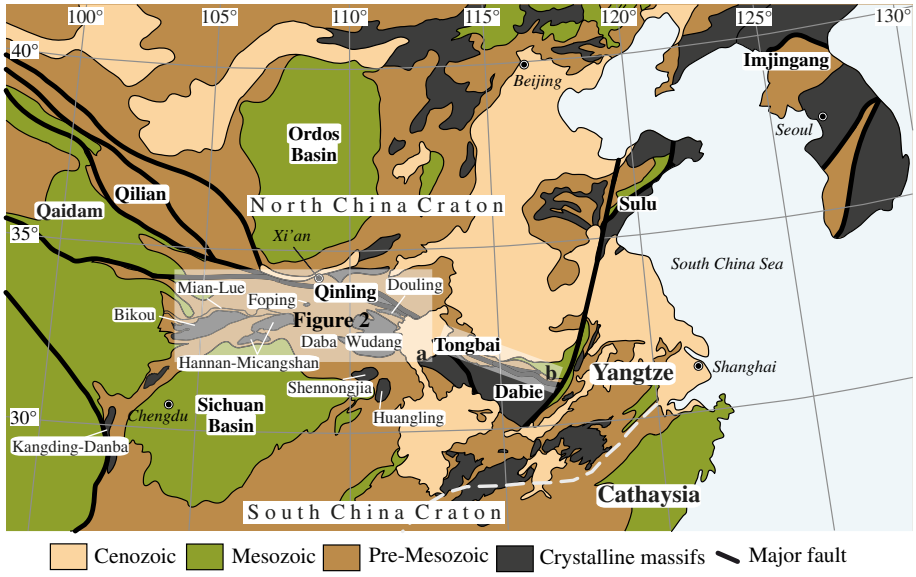

Figure 1. Qilian-Qinling-Tongbai-Dabie-Sulu (herein Qinling-Tongbai) orogenic belt of central China highlighting basement massifs discussed in text. Modified from *Ratschbacher et al.* [2003].

are the Early Paleozoic (U)HP and (U)HT events related tectonically and how do they illuminate the affinities in the Qinling-Tongbai orogenic collage? We argue that a Meso-Neoproterozoic crustal fragment–the Qinling complex–localized several subduction-accretion events that involved ultra-deep accretionary-wedge subduction, mantle-wedge exhumation, back-arc spreading, and spreading-ridge subduction. Finally, we outline along-strike correlations of the Qilian and Qinling segments of the orogen.

2. Characteristics of the Qinling-Tongbai Orogenic Collage: Review and Critical Assessment

[4] In this chapter, we describe the rock units–herein complexes–that are relevant for the Paleozoic Era identified in the Qinling-Tongbai orogen. Between the NCC in the north and the SCC in the south (Figures 1 and 2), these are the continental Kuanping complex, traditionally considered a part of the NCC, the oceanic Erlangping complex, the North-Qinling complex, defined by its UHP mafic and felsic lenses, the Qinling complex, considered a ribbon continent, and the oceanic Danfeng and Songshugou complexes [*Ratschbacher et al.*, 2003; Dong *et al.*, 2011a for recent syntheses]. We provide an assessment of their tectonostratigraphy and magmatic-metamorphic evolution using published U/Th-Pb geochronology (see Table S1 in the supporting information). *Appendix A* explains our data compilation and presentation and gives arguments for the recalculation of some published data sets that are important to our analysis. We refer to part I of this series of papers [*Bader et al.*, 2013] for a summary of U/Th-Pb geochronology and Early Neoproterozoic (~1.0–0.7 Ga) evolution of the Qinling-Tongbai orogenic collage within the Rodinia supercontinent. Throughout the paper, UHP refers to metamorphic processes at pressures high enough to stabilize coesite; UHT stands for crustal metamorphism at temperatures ≥900°C, and ultra-metamorphism (UM) denotes metamorphism involving partial melting of rocks (anatexis or migmatization).

2.1. Kuanping Complex

[5] The Kuanping complex comprises at least two subunits, containing metabasitic (greenschist and amphibolite) and metasedimentary rocks (quartz-rich micaschist and marble). The metabasite unit [e.g., *Zhu et al.*, 2011; *Bader et al.*, 2013] is equivalent to the 1.83–1.73 Ga (median at ~1.77 Ga) Xiong'er magmatic arc rocks [e.g., *He et al.*, 2009] that formed on the southern margin of NCC's Neoarchean-Paleoproterozoic Trans-North China orogen. The metaclastic unit constitutes a remnant of a clastic wedge [*Bader et al.*, 2013] with local Neoproterozoic tholeiitic metabasites [*Diwu et al.*, 2010] that formed during the Grenville orogen. These subunits were affected by ~455–435 Ma (median at ~442 Ma) plutonism and associated ~439–414 Ma (median ~417 Ma) metamorphism (Figure 3), estimated at 570–650°C, 0.66–1.12 GPa in the Tongbai Shan [*Liu et al.*, 2011].

2.2. Erlangping Complex

[6] The Erlangping complex comprises greenschist- to amphibolite-facies metamorphic ultramafic rocks (rare), gabbro, (grano)diorite, pillow lava, sheeted dikes, andesite, rhyolite, Cambrian-Silurian chert (rare), metaclastic rocks (possibly turbidite), and marble [e.g., *Xue et al.*, 1996; *Meng and Zhang*, 2000; *Dong et al.*, 2011a]. A prograde, clockwise P-T evolution (~350°C, ~1.0 GPa to 550–600°C, 0.63–0.77 GPa) was determined in the Tongbai Shan [*Ratschbacher et al.*, 2006; *Liu et al.*, 2011]. Based on geochemical data, the Erlangping complex has been regarded as an intraoceanic arc [e.g., *Xue et al.*, 1996] or back-arc basin [e.g., *Dong et al.*, 2011a]. U-Pb zircon ages span ~4079–359 Ma (Table S1 and Figures 2 and 4a). Mostly mafic metavolcanic rocks and mostly intermediate to felsic metagranitoids group at ~461 and ~430 Ma, respectively; metamorphic zircons and dikes/small intrusions provided the youngest ages (Figure 4a). Sparse Proterozoic inheritance (distinct age groups and single-grain ages, Figure 4a) is at ~2.75, 1.77, 1.15, and 0.92 Ga.

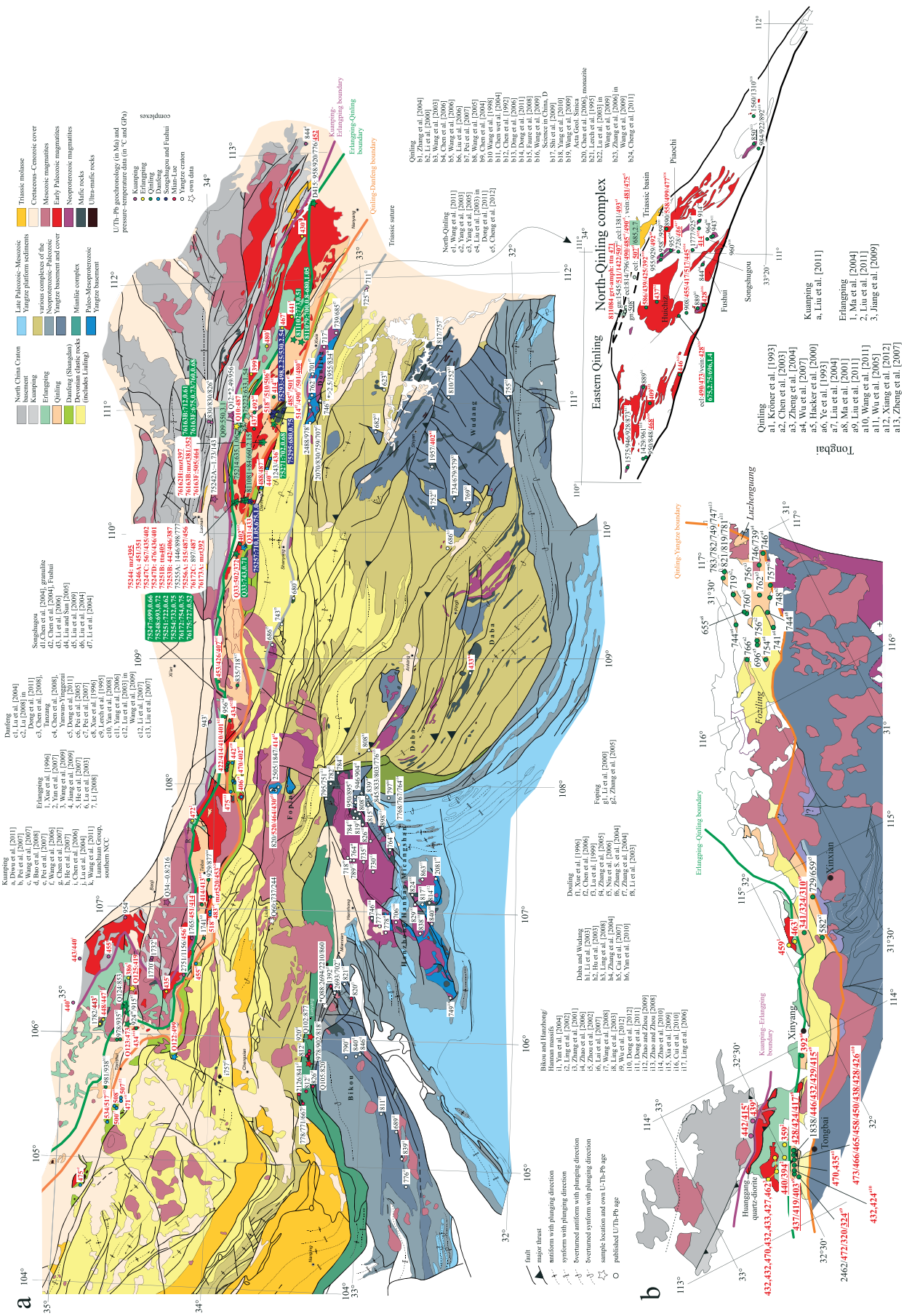

Figure 2.

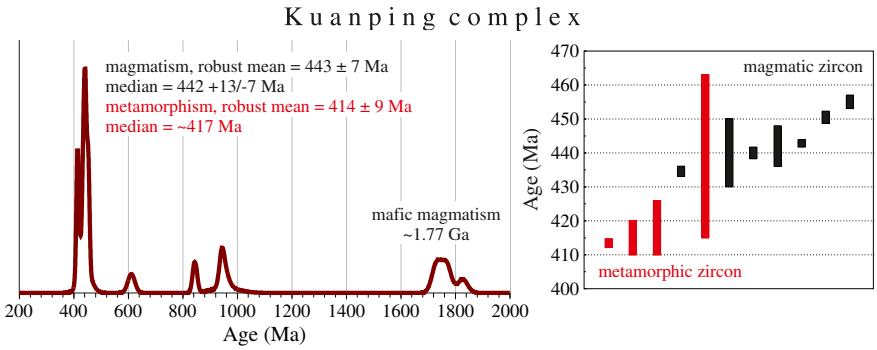

Figure 3. Kuanping complex. (left) U/Th-Pb zircon age probability plot; specific events are highlighted by "robust means" (i.e., Tukey's Biweight Means) [*Hoaglin et al*., 1983] and medians that are used throughout the paper. (right) Discrimination between magmatic and metamorphic zircon ages.

2.3. North-Qinling Complex

[7] Garnet amphibolite and eclogite lenses embedded in quartz-muscovite schist and paragneiss have been grouped into the North-Qinling complex along the northern margin of the eastern Qinling complex; its boundaries and extent (currently <30 km) are unmapped (Figure 2) [e.g., Hu et al., 1995a, 1995b]. Coesite and diamond inclusions in zircon in eclogite and paragneiss indicate UHP metamorphism [*Yang et al*., 2003, 2005; *Wang et al*., 2011a; *Cheng et al*., 2012]. Zircon cores in eclogite and paragneiss, and detrital zircon ages of paragneiss and schist indicate ~1.9–1.7, 1.6–1.4, 1.3–1.0, and 0.8 Ga protoliths and sources (Figure 5a) [*Yang et al*., 2003, 2005; *Wang et al*., 2011a; *Bader et al*., 2013]. Metamorphic zircons date UHP metamorphism at ~515–484 Ma (median at ~497 Ma) and retrograde hydration at ~475 Ma (Figure 5a). This corresponds to 516.4 ± 5.8 and 494.3 ± 2.7 Ma Lu-Hf garnet-omphacite-whole rock ages of two eclogites that formed at peak P-T of 660–710°C, 2.6–2.8 GPa [*Cheng et al*., 2012].

2.4. Qinling Complex

[8] The Qinling complex (Figure 2) comprises siliciclastic and calcsilicate rocks with minor marble and mafic rocks; characteristics are upper amphibolite-facies metamorphism (~700°C, 0.5–0.7 GPa) [*You et al*., 1993], migmatization of felsic gneisses, and intrusion of voluminous granitoids. In the south-central Qinling complex, retrogressed eclogite enclosed in garnet-bearing monzogranite (the southern rim of the Huichizi batholith, Figure 2) yielded 630–720°C, 2.5–3.0 GPa and 696 ± 56°C, 1.4 ± 0.3 GPa for peak and retrograde conditions, respectively [*Cheng et al*., 2011]. In the Tongbai Shan, granulite-facies metamorphism was at 750–805°C, 0.80–0.93 GPa and water activities of 0.10–0.65 [*Liu et al*., 2011; *Bader et al*., 2012a]; armored spinel relics in garnet point to earlier UHT metamorphism at >940°C [*Bader et al*., 2012a; *Xiang et al*., 2012].

[9] U/Th-Pb zircon and monazite ages span ~2462–310 Ma (Table S1), with rare Paleoproterozoic and Mesoproterozoic ages that cover ~1838–1741 and ~1575–1310 Ma. Figures 2, 5b, and 5c subdivide the Qinling-complex U/Th-Pb data regionally, highlight magmatic and metamorphic ages, and delineate specific age groups. In the Qin Mountains (Figure 5c), magmatic zircons define Neoproterozoic (~983–718 Ma) and Paleozoic (~585–392 Ma) groups; the Paleozoic magmatic ages cluster at ~430 Ma (~458–392 Ma) with a break to older ages at ~460 Ma (~499–465 Ma; Figure 5c). Metamorphic zircons and monazites span ~520–402 Ma with most dates at ~420 Ma (Figure 5d); metamorphic zircons in the south-central Qinling complex eclogite show episodic growth at ~490 and ~473 Ma [*Cheng et al*., 2011]. In the Tongbai Shan, most igneous rocks crystallized at ~460 Ma (~473–424 Ma), predating granulite-facies metamorphism at ~430 Ma (~438–415 Ma; Figure 5b) [e.g., *Liu et al*., 2011]. Taking conservative brackets, the published ages indicate ≥110 Myr (500–390 Ma) of Paleozoic magmatism; a possible eastward-younging trend is weak and similar to that in the other complexes of the Qinling-Tongbai orogenic collage (Figure 5e).

[10] To better reveal the range of magmatism in the Qinling complex, we recalculated the ages and derived distinct concordia-age groups (see Appendix A) from the orthogneiss data of *Wang et al*. [2009]; in part, these granitoids constitute the largest batholiths of the Qinling complex (Huichizi, Piaochi, Figure 2). Consistent with findings in other magmatic terranes [e.g., *Glazner et al*., 2004], the Qinling-complex intrusions contain magmatic zircons best interpreted as inherited from multiple intrusion cycles. The Huichizi batholith (Figure 5f) records crystallization

Figure 2. Correlation of Paleozoic and older rock units ("complexes") in the Qinling-Tongbai orogen, distribution of plutons, trend of mostly Triassic fold trains and faults, and distribution of Paleozoic and Precambrian U/Th-Pb ages detailed in Table S1 (supporting information) and *Bader et al.* [2013] (with references). Our new data are given with leading sample number; underlined are metamorphic zircon ages; mzt, monazite; ttn, titanite; data with "*" denote major detrital age clusters, and "i" indicates that the age is an inherited zircon population in a younger rock. New pressure-temperature data with leading sample number are in white, underlain by green and blue shades, asserting them to the various complexes. Map adapted from 1:1,000,000 Geologic and Tectonic Maps of the Qinling-Daba Mountains [*Zhang*, 1992; *Zhang et al.*, 2001]. A more detailed geologic evaluation is prohibited by the unavailability of 1:200,000 maps to the geologic community outside of China.

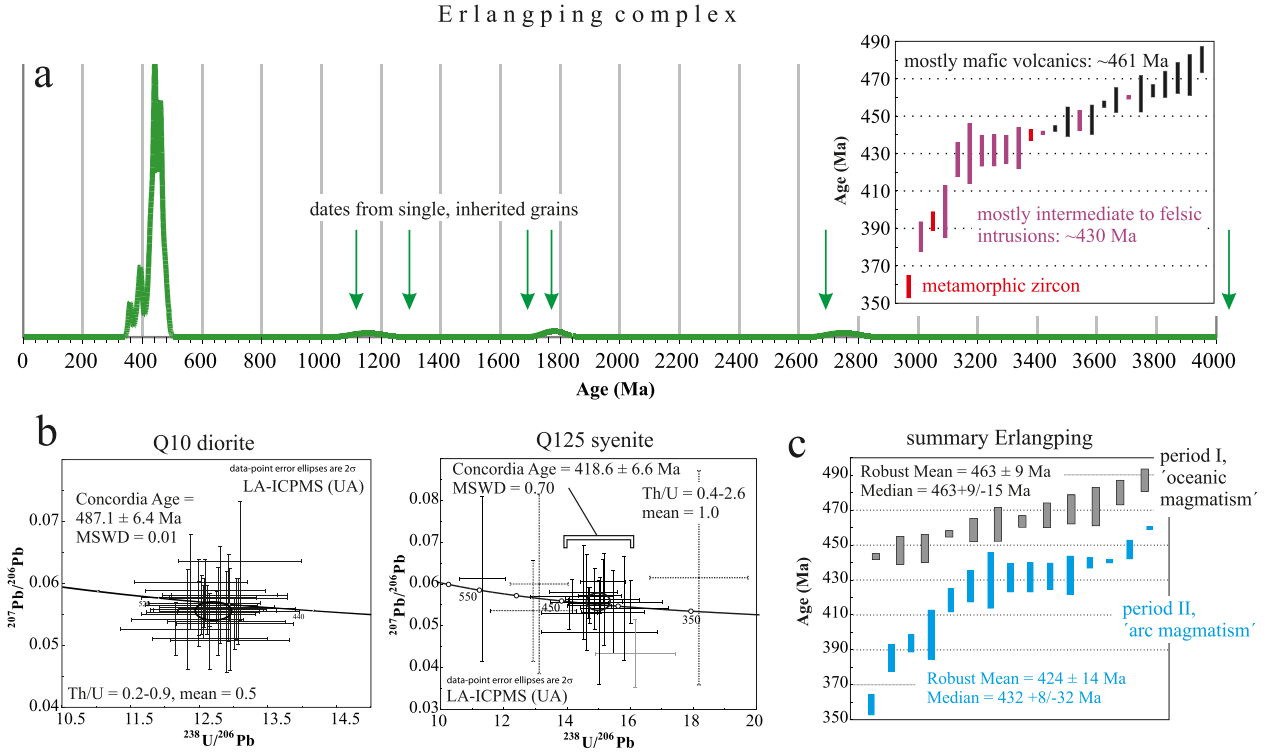

Figure 4. Erlangping complex. (a) U/Th-Pb zircon age probability plot and discrimination between ages from mostly mafic (black) and mostly intermediate-felsic (magenta) igneous rocks; metamorphic zircon ages in red. (b) New U/Th-Pb zircon data. (c) Summary of all U/Th-Pb zircon data and suggested subdivision into an early intraocean arc–back-arc ("oceanic") period and a later arc stage; see text for discussion.

events at ~425, ~439, and ~586 Ma; inherited zircons sample the Neoproterozoic magmatism of the Qinling complex. In the Piaochi batholith, crystallization cycles span ~80 Myr (~478 final crystallization, 499, 558 Ma), with inheritance (~890, 1115 Ma) characteristic for its host paragneiss [*Bader et al.*, 2013]. The volumetrically smaller Neoproterozoic igneous rocks provide evidence for Paleozoic and Mesozoic and reheating (~165, 452, 480 Ma) [e.g., *Shi et al.*, 2009; *Bader et al.*, 2013].

2.5. Danfeng and Songshugou Complexes

[11] The Danfeng complex (Figure 2) comprises greenschist-facies Cambrian-Silurian chert, ultramafic and mafic rocks, pillow lavas, and intermediate-acidic intrusions; the mafic rocks have MORB and island-arc/continental arc trace-element signatures [e.g., *Xue et al.*, 1996; *Yan et al.*, 2008; *Dong et al.*, 2011b]. U-Pb zircon ages span ~534–402 Ma, with a single upper intercept age of ~1243 Ma; most mafic and intermediate rocks are ~534–470 Ma (median ~494 Ma) and 455–402 Ma (median ~436 Ma; Figure 6a), respectively.

[12] The ~25 × 5 km Songshugou complex (Figure 2) has an elliptical core of dunite and subordinate harzburgite and wehrlite and a serpentinized rim, which is surrounded by fine-grained amphibolite that hosts lenses of coarse-grained amphibolite with plagioclase corona around relic garnet porphyroblasts, HP mafic granulites, and some felsic granulites [e.g., *Zhang*, 1999; *Dong et al.*, 2008]. The mafic granulites evolved from a possible eclogite stage to documented peak metamorphism at 830–920°C, 1.0–1.6 GPa, and to ≤700°C, 0.6–0.9 GPa [*Liu et al.*, 1995, 1996; *Zhang*, 1999]. Geochemical data indicate MORB metabasites [*Liu et al.*, 2004; *Dong et al.*, 2008]. In contact with the Songshugou, Danfeng, and Qinling complexes are the Fushui intrusions that comprise metamorphosed gabbro, diorite, and sparse tonalite, monzonite, and ultramafic rocks; geochemically, they comprise tholeiitic and calc-alkalic magmatites [*Dong et al.*, 1997a; *Zhang*, 1999].

[13] Sm-Nd mineral and whole-rock metabasite isochrons have been used to approximate the formation age of the Songshugou complex [*Li et al.*, 1991; *Dong et al.*, 1997b, 2008]. Figure 6b replots the (garnet) amphibolite whole-rock data. From these, *Dong et al.* [1997b, 2008] selected five and obtained a ~1030 Ma isochron; all available data yield ~843 Ma, a selection of four ~762 Ma, and three give ~413 Ma. Although the ages appear geologically meaningful in the context of Qinling geochronology (section 2.4) [*Bader et al.*, 2013], the dates may at best indicate a mixture of Neoproterozoic and Paleozoic components. U-Pb zircon and baddeleyite ages from gabbro and monzonite of the Fushui intrusions yielded magmatic dates of 514–490 Ma with one metamorphic date of ~480 Ma (Figure 6c). The Songshugou garnet-amphibolite zircons show features typical of metamorphic zircons; their U-Pb ages span 518–506 Ma [*Liu and Sun*, 2005; *Liu et al.*, 2009]. Two mafic granulites yielded 501–485 Ma metamorphic zircons (Figure 6c) [*Chen et al.*, 2004; *Su et al.*, 2004].

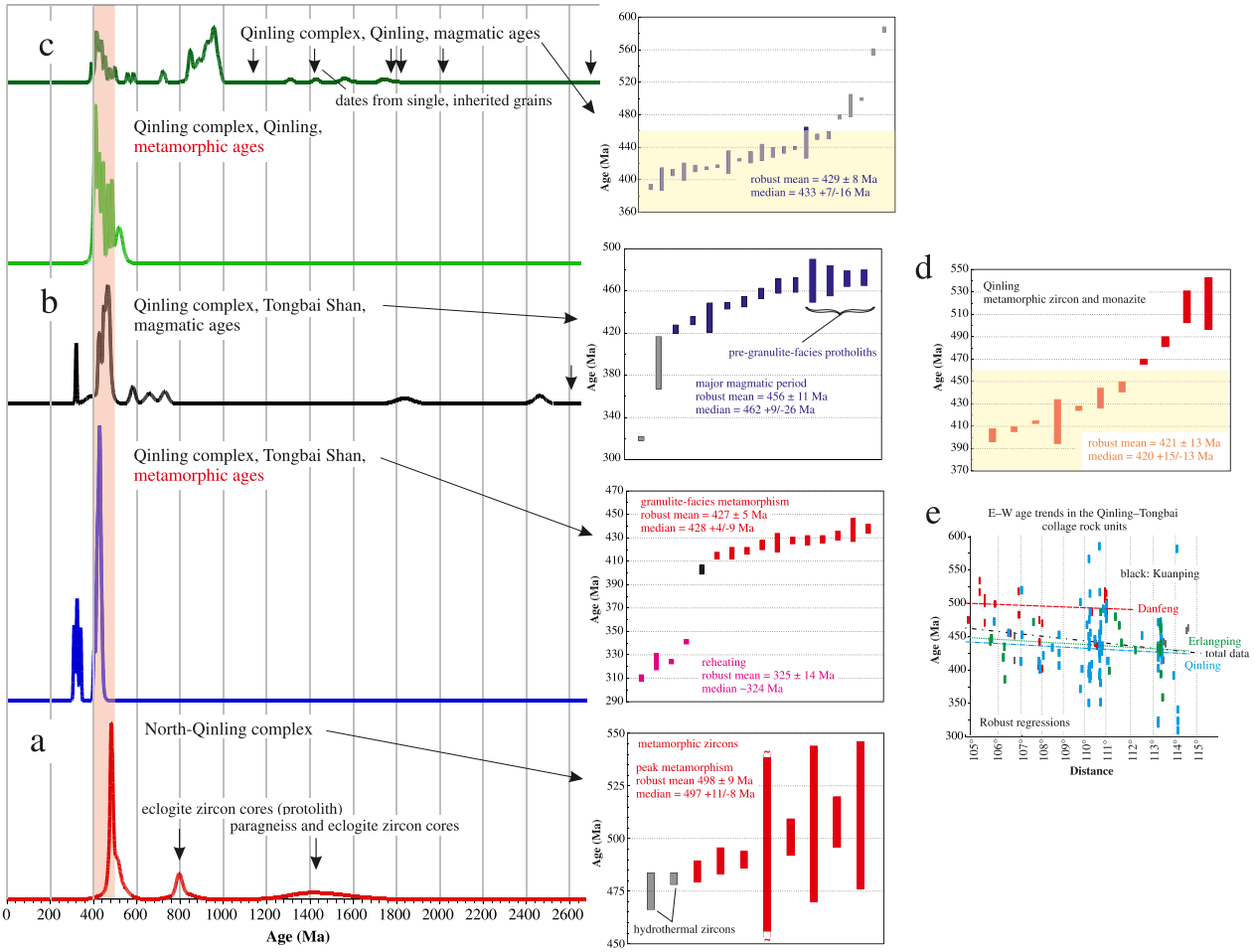

Figure 5. (a–c) U/Th-Pb zircon and monazite age probability plots normalized by the number of analyses (i.e., each curve contains the same area) for the North-Qinling complex and the Tongbai Shan and Qinling areas of the Qinling complex; specific events are highlighted to the right. (d) Metamorphic zircon and monazite from the Qinling complex. (e) Analysis of possible along strike age trends in the Qinling complex and comparison with the other complexes of the Qinling orogenic collage. (f) *Wang et al.*'*s* [2009] Huichizi and Piaochi granite batholith zircon data, recalculated and replotted to highlight multiple intrusion cycles; these granitoids represent some of the largest Paleozoic intrusions in the Qinling complex. (g) New U-Pb titanite and ^{40}Ar-^{39}Ar phengite ages from the North-Qinling complex, dating post UHP cooling. (h) New U-Pb zircon ages from the Qinling complex. (i) New U-Pb zircon and Th-Pb monazite ages from N-S profile across the southern central Qinling complex in the East-Qinling; see Figure 2 for location. (j) As in Figure 5i but in the western East-Qinling. (k) As in Figure 5i but in the southwestern East-Qinling. (l) Lithology-age-metamorphism relationships of our new P-T-time data from N-S profiles across the Qinling complex; see text for discussion.

2.6. South China Craton

[14] The SCC is traditionally subdivided into the Yangtze and Cathaysia blocks (Figure 1). The core of the Yangtze block is exposed in the Kongling area (Huangling dome) [e.g., *Gao et al.*, 2011] and yielded, along with the Dabie and Douling complexes (Figures 1 and 2; Huangtuling granulite) [e.g., *Wu et al.*, 2008], Archean-Paleoproterozoic ages. This core was split and reassembled during the Grenville orogeny (Miaowan "ophiolite"—Shennongjia arc association) [*Peng et al.*, 2012; *Bader et al.*, 2013], and trench–fore-arc–arc complexes (Mian-Lue–Bikou-Hannan-Micangshan and Kangding-Danba assemblages; Figures 1) were accreted to this nucleus during the Neoproterozoic (Figure S1 in the supporting information) [*Bader et al.*, 2013]. Overlying the crystalline basement is ~12 km of Upper Sinian to Triassic sedimentary rocks [e.g., *Ratschbacher et al.*, 2003, and references therein]; the Cambrian through Carboniferous strata formed on the north-facing Yangtze-block passive margin.

[15] In the Cathaysia block (Figure 1), Phanerozoic, particularly Mesozoic, igneous, and sedimentary rocks prevail; Precambrian basement rocks are locally exposed along its central, NE-striking axis. Neoproterozoic igneous rocks and Late Neoproterozoic–Early Paleozoic passive margin sedimentary rocks occur on both the Yangtze and Cathaysia blocks [e.g., *Li et al.*, 2008b]. The Cathaysia block contains the Early Paleozoic Wuyi-Yunkai (or Kwangsian) orogen, in which magmatism and metamorphism peaked

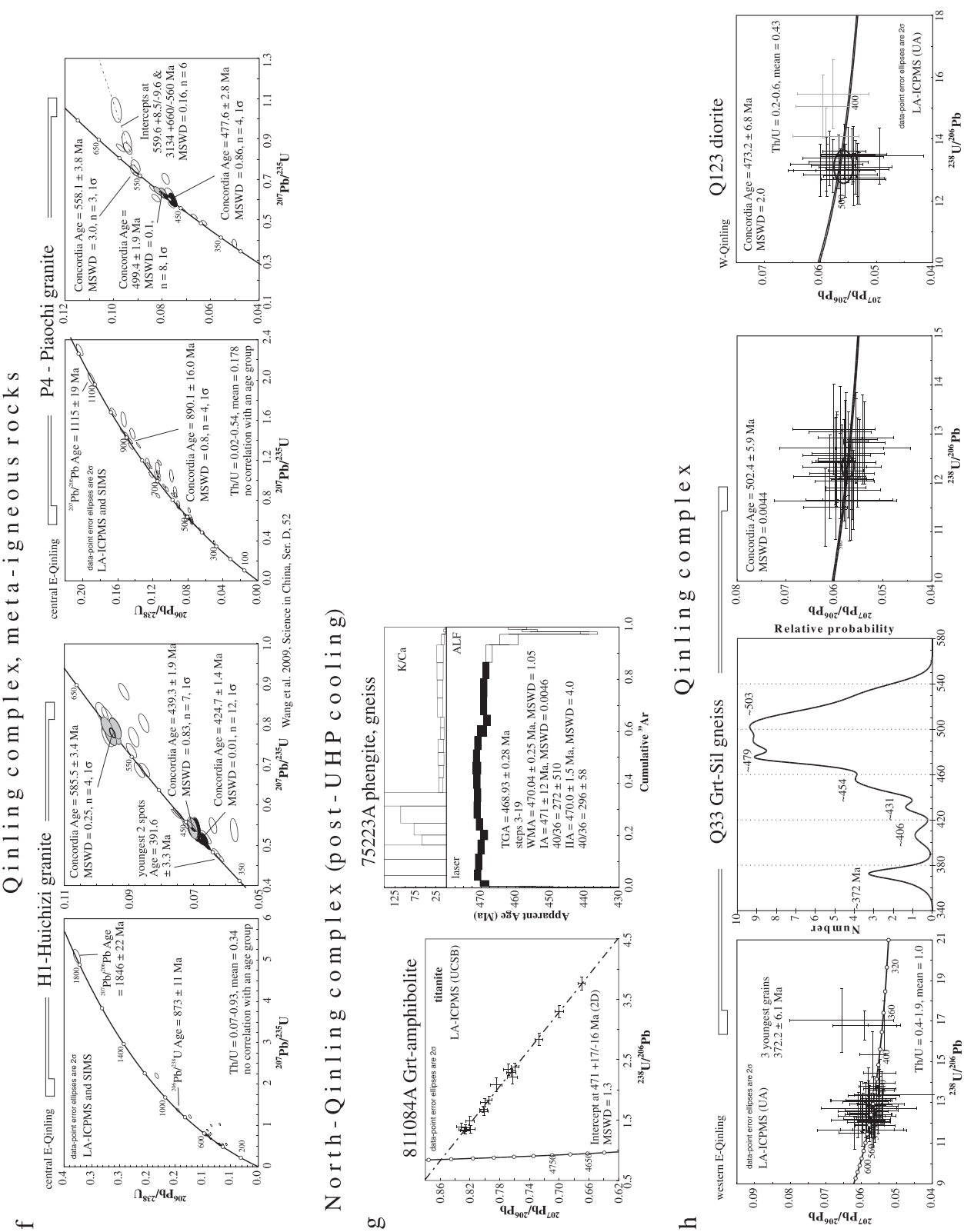

Figure 5. (continued)

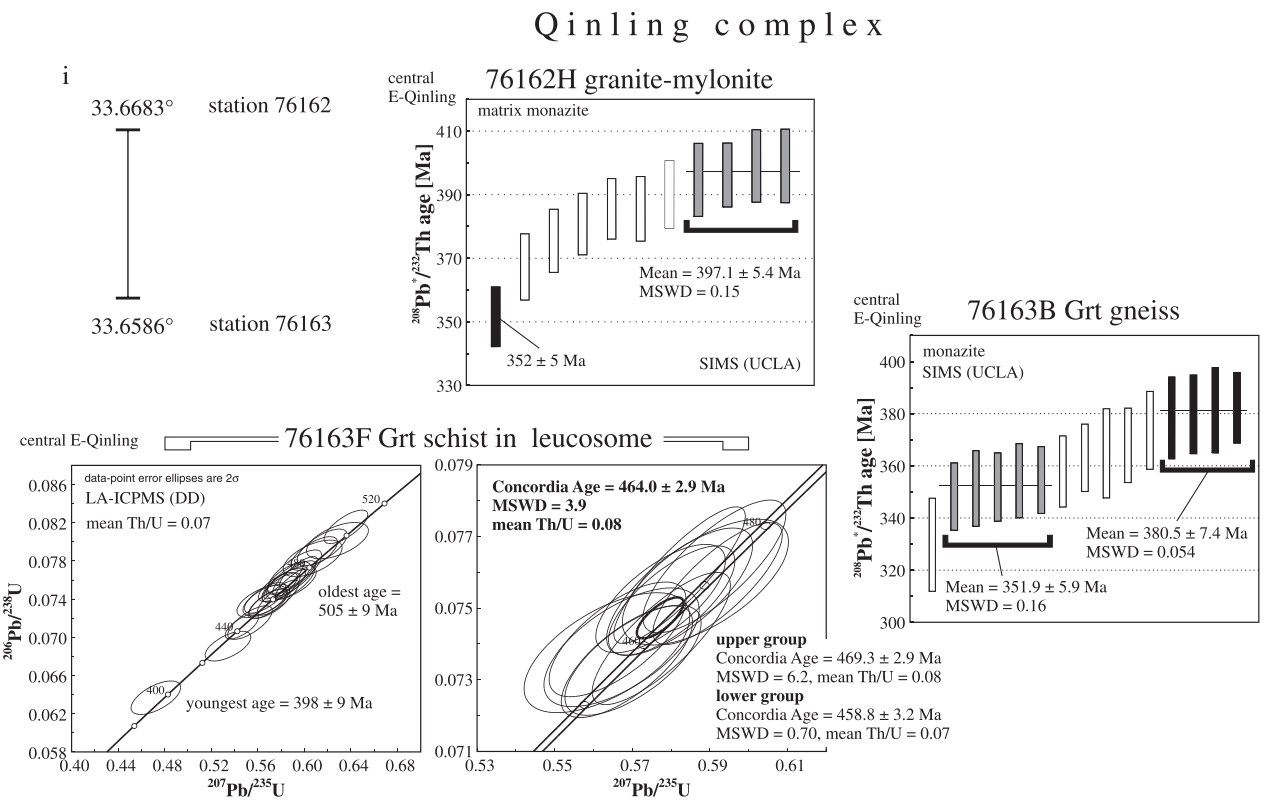

Figure 5. (continued)

at ~460–410 Ma (median ~438 Ma; Figure S1). Although controversial, this orogen may have originated from inversion of a Neoproterozoic–Early Paleozoic failed rift [e.g., *Wang et al*., 2011b].

[16] In the Yangtze block, Early Paleozoic sills and a dike swarm in the Daba and Wudang Shan (Figure 1) [*Ratschbacher et al*., 2003] have been interpreted to record plume-induced rifting [e.g., *Xu et al*., 2008]; some eclogites and gneisses in the Dabie Shan and the Foping dome (Figure 1) may have similar protoliths. This rare magmatism spans 579–402 Ma with most ages at ~445 Ma (Figure S1).

3. New Petrology and New Geochronology

[17] Our new petrology and geochronology aim to elucidate further the Early Paleozoic characteristics of the Qinling-Tongbai orogenic collage, i.e., the peak and retrograde metamorphic conditions and regional distribution and age of magmatism and metamorphism. Appendix S1 (supporting information) explains the methods employed. Table S2 (supporting information) summarizes the locations and characteristics of the analyzed rocks. Tables S3–S11 (supporting information) compile the analytical data of this study. The following paragraph provides a concise summary of our findings allowing the reader a rapid access to the subsequent discussion.

[18] We show that the North-Qinling complex mafic rocks record UHP metamorphism at ~550°C, 3.1 GPa and reequilibration during exhumation at ~660°C, 2.0–2.3 GPa; the felsic gneisses reequilibrated at ~635°C, 1.5–1.1 GPa. The P-T data of paleosomes, melanosomes, and leucosomes of the Qinling complex highlight upper amphibolite-facies metamorphism. Partial melting of felsic gneisses started at 660–700°C, in a P range of 0.5–0.8 GPa. Garnet-core isopleth thermobarometry yielded 675–773°C and 0.51–0.75 GPa (median at ~717°C, 0.68 GPa). Prograde and retrograde garnet growth histories covered ~675°C, 0.73 GPa to ~760°C, 0.68 GPa and ~700°C, 0.80 GPa to ~680°C at 1.05 GPa, respectively. The ultramafic and mafic rocks of the Songshugou complex yielded 650–710°C, <0.8 GPa. The garnet-amphibolite mantle of the Songshugou ultramafic rocks gave a prograde P-T path, ~498°C, 2.25 GPa to ~530°C, 2.54 GPa and subsequent heating to 660–700°C, 1.1–1.2 GPa. Spinel-peridotite in the western East-Qinling complex, attributed to the southerly abutting Danfeng complex and correlated with the Songshugou ultramafic rocks farther east, yielded 680–740°C, <1.1 GPa.

[19] Our new dates support the subdivision of the Erlangping-complex magmatism into an older more mafic and a younger more felsic rock assemblage and extend its onset to ~490 Ma. U-Pb titanite and ^{40}Ar-^{39}Ar phengite dates imply that the North-Qinling complex UHP rock had reached middle-upper crustal depths at ~470 Ma. Qinling-complex magmatism is characterized by a continuous activity spanning at least 515–400 Ma; amphibolite protoliths have both Neoproterozoic and Early Paleozoic ages; migmatization is long lasting but terminated at ~400 Ma, coeval with synkinematic intrusions and HT mylonitization; reheating occurred at ~360 Ma. Our dates for the early more mafic rock group in the Danfeng complex stem from the Western Qinling and yielded ~500 Ma crystallization and detrital age groups at ~0.8, 0.96, and 1.1 Ga, typical for the

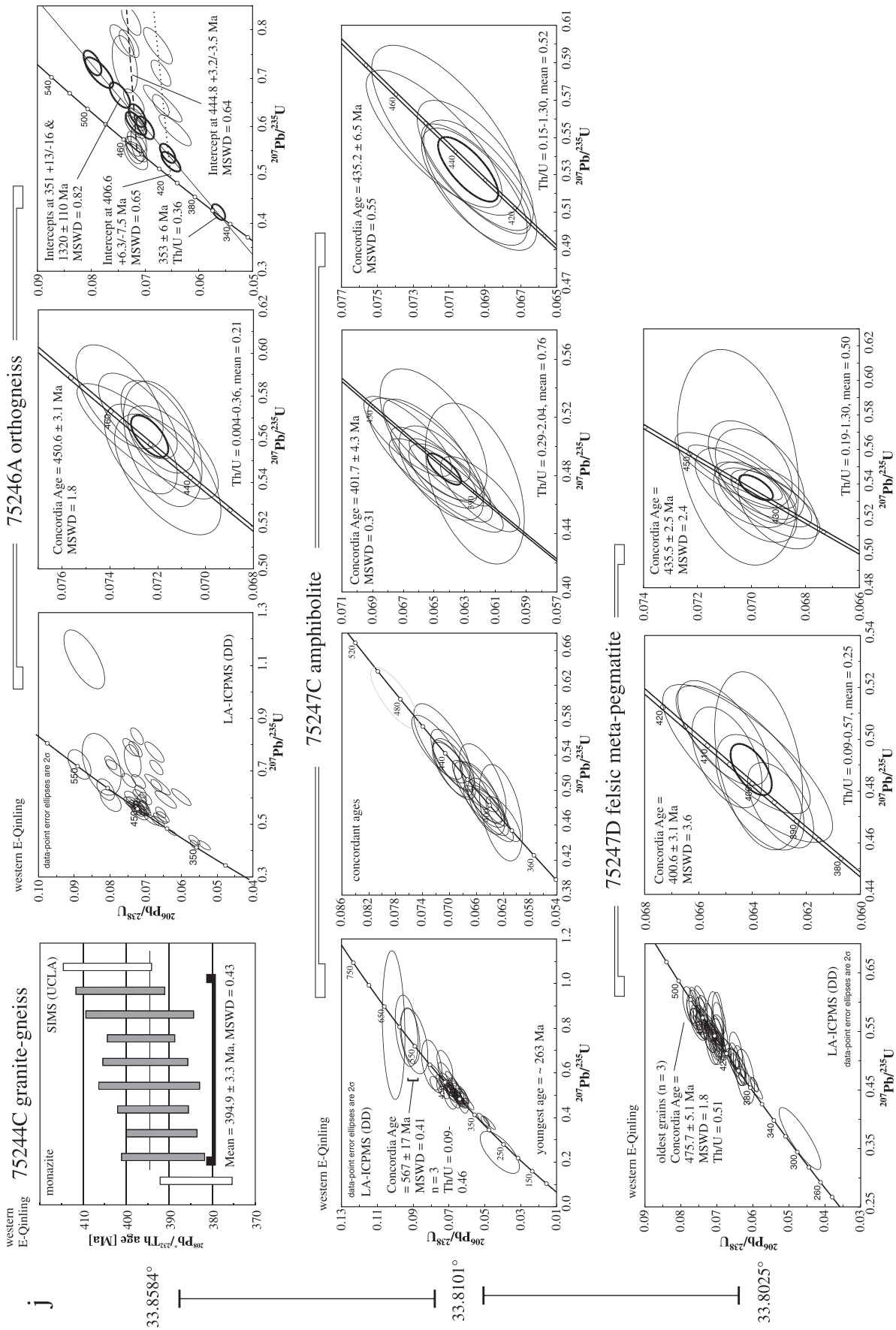

Figure 5. (continued)

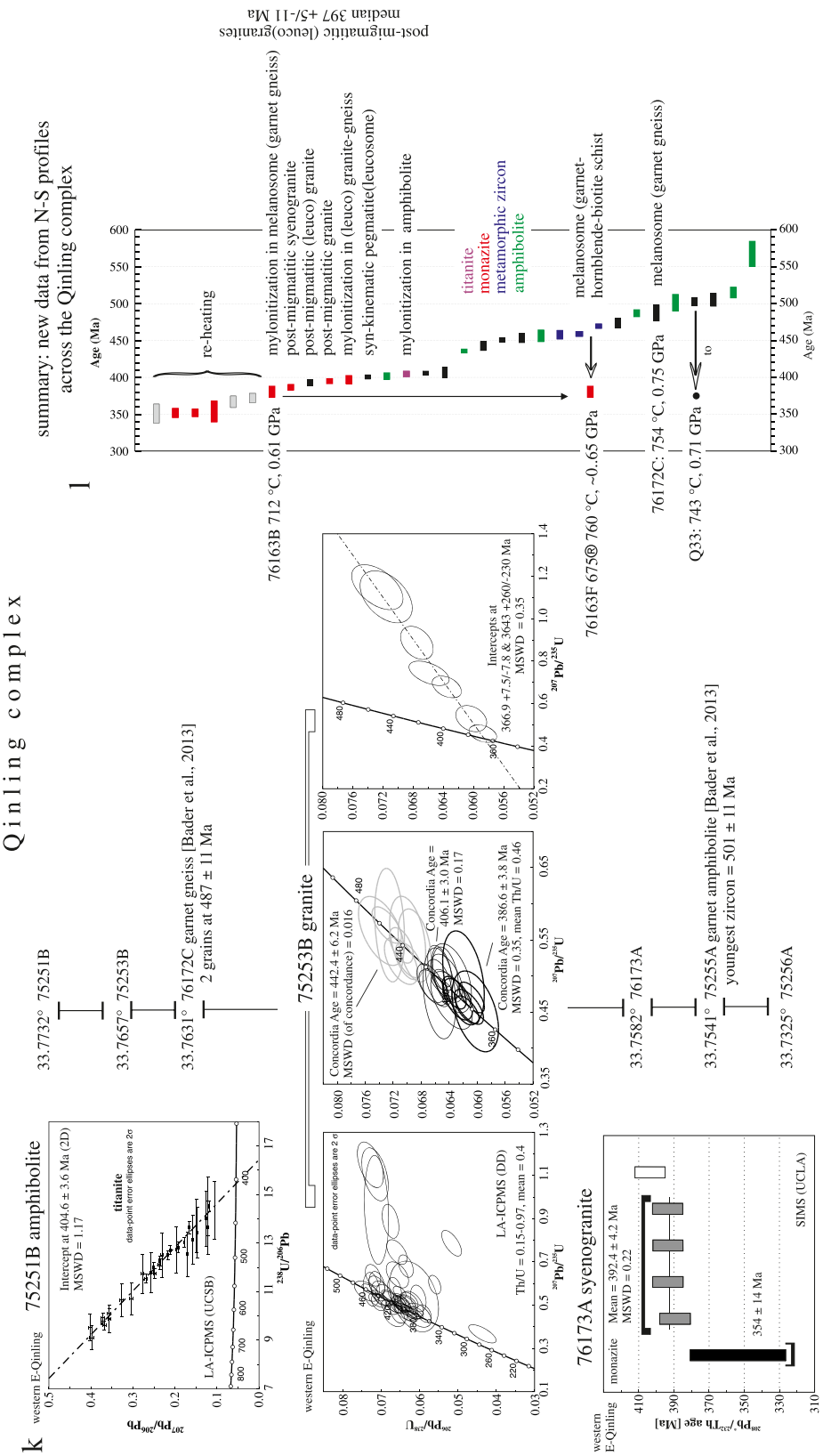

Figure 5. (continued)

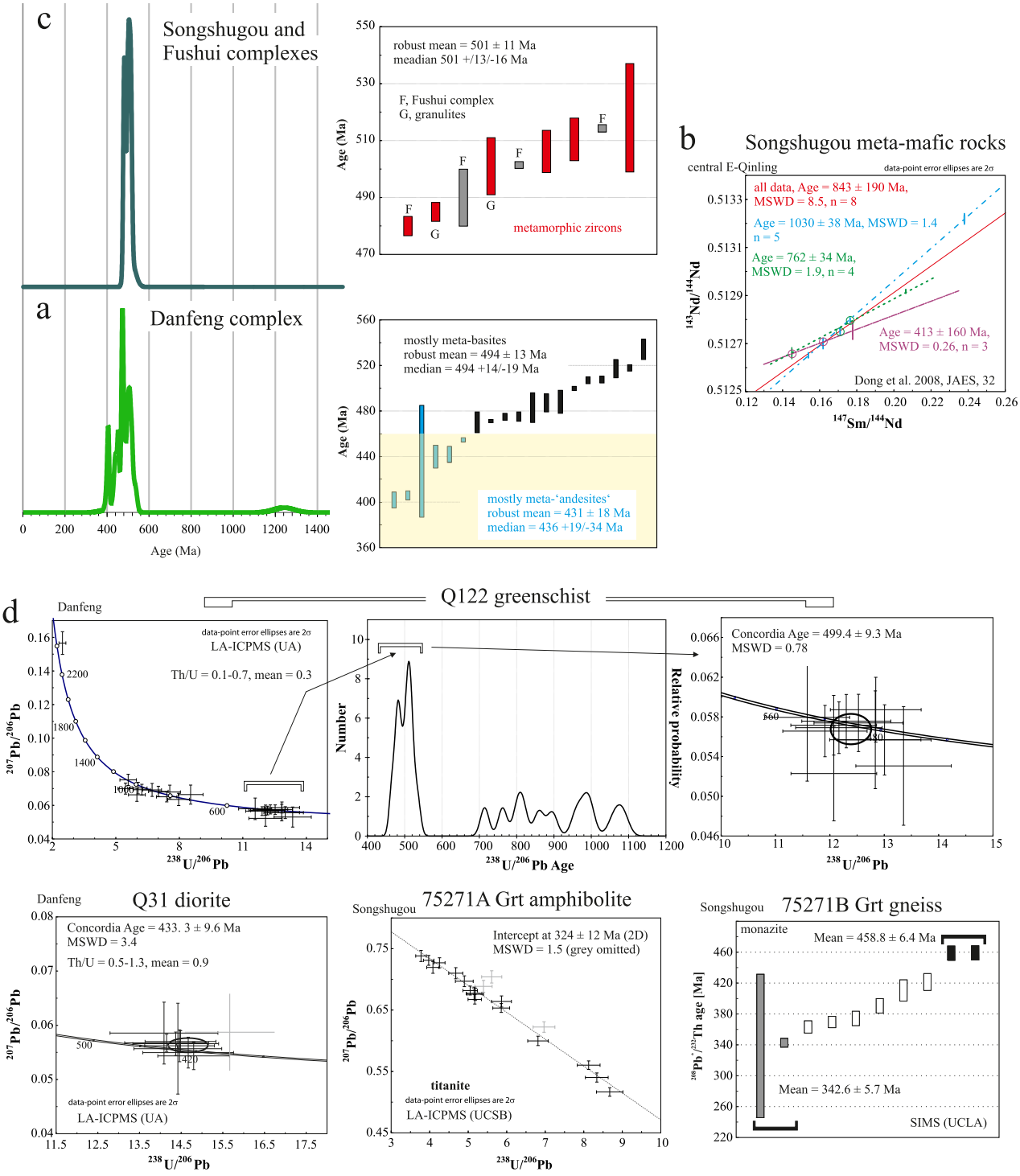

Figure 6. (a and c) As in Figures 5a–5c but for the Danfeng and Songshugou-Fushui complexes. (b) Sm-Nd (garnet) amphibolite whole-rock data of the Songshugou metamafic rocks, replotted and recalculated from *Li et al*. [1991] and *Dong et al*. [1997b, 2008]. (d) New zircon and titanite U-Pb and monazite Th-Pb ages from the Danfeng and Songshugou complexes.

Neoproterozoic evolution of the Qinling orogenic collage; the younger, more felsic rock group intruded at ~435 Ma. We constrain the retrograde path of the Songshugou-complex rocks by Th-Pb monazite and U-Pb titanite ages to ≥459 Ma, with reheating at ~343–324 Ma.

3.1. North-Qinling (U)HP Metamorphic Rocks: Petrography and Phase Equilibria

[20] We investigated a succession of garnet-bearing gneiss with intercalated marble and associated fine- to medium-grained eclogite and garnet amphibolite (likely retrogressed

eclogite), which form lenses and boudins meters to several hundred meters in length.

3.1.1. Metabasite

[21] The eclogite-facies UHP-HP assemblage comprises garnet cores, omphacite, coesite/quartz, and rutile. Retrogression comprises the decomposition of omphacite, amphibole growth, formation of interstitial plagioclase, and transformation of rutile to titanite and ilmenite. While most metabasites bear anhedral and fragmented garnets (e.g., 811081A, Figure S2a), eclogites Q09B and 811084A have euhedral garnet porphyroblasts (≤1 mm) with calcite, quartz, rutile, apatite, kyanite (Q09B), pyrite, and pyrrhotite inclusions. Some garnets (811084A) show radial cracks around quartz inclusions, suggesting the former presence of coesite [cf. *Hu et al*., 1995a]. Q09B garnets have a core section with a composition of $Alm_{53}Grs_{34}Prp_{11}Sps_2$, followed by a concentric intermediate zone with maximum grossular and minimum pyrope content, and rims with strongly increasing pyrope content ($Alm_{53}Grs_{31}Prp_{15}Sps_1$; Figure 7a and Table S3). A few 811084A garnets have a small core of $Alm_{55}Grs_{31}Prp_{12}Sps_2$, a pyrope-poor inner rim of $Alm_{62}Grs_{29}Prp_8Sps_1$–equal to the core composition of other garnets–and an outer rim of $Alm_{55}Grs_{27}Prp_{16}Sps_2$ (Figure 7a). Weakly zoned 811081A garnets average $Alm_{56}Grs_{27}Prp_{16}Sps_1$ (Figure 7a and Table S3). Relic omphacite prisms in Q09B, 811081A, and 811084A have jadeite contents between 25 and 35 mol% (Table S4) and most are surrounded by symplectites of albite, quartz, and omphacite with jadeite contents of 12–22 mol% (Figures S2a–S2c). The 811081A phengite forms small, subhedral flakes (Figure S2d) with high Si contents of 3.36 per formula unit (p.f.u.) and X_{Mg} of 0.69 (Table S5). Calcic amphibole shows compositions along the pargasite-edenite or tschermakite-magnesiohornblende joins (Table S6); in Q09B, core to rim, X_{Mg} decreases from 0.75 to 0.69 and Ti increases from 0.05 to 0.08 p.f.u., implying rising T during growth. Zoning is similar in 811081A: X_{Mg} is 0.56–0.50 and Ti is 0.08–0.12 p.f.u. Unzoned 811084A amphibole has X_{Mg} values and Ti contents of 0.52 and 0.10 p.f.u., respectively. Interstitial plagioclase (Q09B, 811081A) has clinozoisite inclusions; its composition is constant within thin sections but varies from $Ab_{97}An_{03}$ to $Ab_{87}An_{13}$ among the investigated samples (Table S7).

[22] The garnet zoning and the ubiquitous relic phases record chemical disequilibria, prohibiting thermodynamic modeling due to difficulty in choosing an appropriate bulk-rock composition. We obtained thermobarometric information on the UHP stage from eclogite Q09B using multiequilibrium calculations. Assuming that relic kyanite was in equilibrium with kyanite-bearing garnet, matrix omphacite with the highest jadeite content, and SiO_2, winTWQ calculations yielded ~550°C, 3.1 GPa (Figure 7b), in accord with the presence of diamond inclusions in zircon [*Yang et al*., 2003]. Conventional thermobarometry [*Krogh Ravna and Terry*, 2004], using the 811081A assemblage phengite-omphacite-garnet-quartz, yielded ~660°C, 2.0–2.3 GPa; this likely records reequilibrium of these phases during exhumation. The method in general has a higher uncertainty than other conventional thermometers due to Fe^{3+} in clinopyroxene and phengite.

3.1.2. Felsic Gneiss

[23] Garnet-bearing phengite gneiss 75223A displays aligned coarse phengite bending around millimeter-sized albite porphyroblasts. Anhedral 80–200 μm garnet (Figure S2e) is pristine where included in albite or phengite and chloritized in the matrix. Biotite grew along phengite grain boundaries and cracks. Garnet and matrix ilmenite encase relic rutile. Other accessories include ≤0.5 mm euhedral tourmaline, zircon, apatite, and pyrite. Garnet shows increasing grossular and decreasing almandine contents from core ($Alm_{74}Prp_9Grs_{15}Sps_2$) to rim ($Alm_{71}Prp_{7\text{-}8}Grs_{19}Sps_{2\text{-}3}$; Figure 7c and Table S3). Albite porphyroblasts ($Ab_{94\text{-}97}An_{03\text{-}06}$) locally show oligoclase rims of $Ab_{80}An_{20}$. Phengite has Si contents of 3.26–3.32 p.f.u. and X_{Mg} values of 0.52 and 0.58; higher X_{Mg} values correspond to higher Si contents. Biotite is unzoned with X_{Mg} of 0.54 and X_{Ti} (=Ti/octahedral sum) of 0.027 (Table S8). 75223A garnet isopleths calculated in the NCKFMASHT system intersect at ~633°C, 1.5 GPa, in the stability field of the assemblage garnet-plagioclase-omphacite-phengite-paragonite-biotite-quartz-rutile (Figure 7d), matching the observed assemblage—except for paragonite and omphacite, whose absence from the rock may reflect decomposition during further cooling. X_{An} isopleths of albite and the Si content of phengite substantiate pressure (Figure S3). The intersection of the garnet-core with the Si-in-phengite isopleths within this divariant field, which is characterized by the continuous decomposition of omphacite and formation of plagioclase, reflects recrystallization. There was late decomposition of rutile to ilmenite, and the formation of An_{20} rims on albite.

[24] Garnet-bearing gneiss 75214D, ~10 km west of 75223A, consists of garnet, plagioclase, quartz, biotite, and accessory ilmenite, apatite, and zircon (Figure S2f). Garnet is discontinuously zoned (Figure 7e and Table S3) with cores of $Alm_{54}Grs_{20}Prp_{09}Sps_{17}$ and rims of $Alm_{61}Grs_{14}Prp_{09}Sps_{16}$. Plagioclase is $Ab_{74}An_{26}$ (Table S7). Biotite has X_{Mg} of 0.50 and X_{Ti} of 0.028–0.034 (Table S8). Modeling in the NCKFMASHT system with excess H_2O yielded an intersection of garnet-core isopleths at ~635°C, 1.1 GPa, in the stability field of the assemblage garnet-plagioclase-biotite-phengite-quartz-ilmenite (Figures 7e and S4); phengite, not observed in thin section, likely decomposed during cooling.

3.2. Qinling-Complex Ultrametamorphic Rocks: Petrography and Phase Equilibria

[25] Many Qinling-complex rocks underwent UM overprint; especially felsic gneisses experienced anatexis, with the formation of quartz–feldspar-rich layers (leucosome) and melt-depleted sections (melanosome) [Mehnert, 1968]. Virtually unaltered protoliths and moderately modified gneisses comprise paleosome. The migmatites are either folded or stromatitic (Figure S2g). The degree of partial melting increased southward, evident in increasing amounts of leucosome. Anatexis is absent in ~1–100 m, mafic lenses and boudins; ≥5 mm thick zones enriched in garnet and biotite developed along the metabasite-leucosome contacts (Figure S2h).

[26] Our profiles across the southern Qinling complex, either into rocks mapped as the Danfeng (southwestern East-Qinling, Figure 2) or the Songshugou-Fushui complexes (central East-Qinling), do not show clear complex boundaries; in contrast, gneisses (melanosomes) are intercalated with (garnet) amphibolites (paleosomes) and both are invaded by leucosomes and granitoids. We suggest that the investigated gneiss-amphibolite (local ultrabasite)-migmatite association

comprises (ultra)mafic rocks of the Songshugou-Fushui and Danfeng complexes and gneiss-metabasite intercalations, characteristic of the southern Qinling complex, blurred by HT metamorphism, migmatization, and magmatism. This transitional nature of complex boundaries may reflect the tectonic setting (see section 4).

3.2.1. Fabrics and Mineral Compositions of Paleosomes, Melanosomes, and Leucosomes

[27] Garnet-biotite gneiss paleosomes consist of garnet, biotite, plagioclase, quartz, and local sillimanite and K-feldspar (Figures S2i and S2j). Rare Fe-Mg-Mn amphibole (Figure S2k) joins the peak-metamorphic assemblage. Muscovite is a common retrograde phase (Figure S2l). Accessories include ilmenite, apatite, zircon, monazite (Figure S2m), and rare xenotime (sample 75248C, identified by Raman spectroscopy). Textures vary among samples: garnet gneiss 75247F (Figure S2n) is massive, granular, and medium grained with decussate biotite aggregates; in 75248C, 75251E, 75271B, and 811079A, euhedral biotite and muscovite crosscut anastomosing domains. Compositional banding in gneiss 75254A comprises garnet-biotite-plagioclase-quartz, plagioclase-quartz, and cummingtonite-plagioclase-quartz layers.

[28] Melanosomes are enriched in garnet and biotite, producing compositional layers of biotite-plagioclase-quartz and garnet-biotite-plagioclase-quartz (e.g., 76172C, 811102F, Figure S2o). Mylonites have a matrix of dynamically recrystallized quartz and fine-grained biotite with clasts of garnet and plagioclase (e.g., 76172C, Figure S2p). Paleosomes and melanosomes contain mostly anhedral, 0.2–2.0 mm garnet with low grossular (4–9 mol %), high almandine (63–79 mol%), and variable (5–24 mol%) pyrope and spessartine contents. The grossular content is constant across most grains; local distinctly rimward increasing spessartine and decreasing pyrope contents reflect retrogression (e.g., 75251E and 75254A in Figure 8 and Table S3). In contrast to other garnets from felsic migmatites, garnet of gneiss 811079A shows elevated grossular contents in the core ($Alm_{63}Grs_{15}Prp_9Sps_{13}$) and discontinuous increase of grossular in the rims ($Alm_{58}Grs_{27}Prp_7Sps_8$; Figure 8). Weakly zoned or unzoned plagioclase has anorthite contents of 22–40 mol% (Table S7); most grains include randomly oriented sillimanite needles. K-feldspar has an albite content of ~9 mol%. Reddish-brown biotite has high X_{Ti} values of 0.045–0.100; the highest occur in the cores of large flakes; X_{Mg} values (0.35–0.65) vary among samples (Table S8). Late euhedral muscovite, often intergrown with biotite, cuts the foliation or mantles sillimanite (e.g., 75251E, Figure S2l); the grains have variably low Si contents of 3.00–3.13 p.f.u. and X_{Mg} values of 0.35–0.48. Euhedral, randomly oriented cummingtonite [*Leake et al*., 1997] occurs in layers (75254A, Figure S2k) and has an X_{Mg} value of 0.55 (Table S6); relic magnesiohornblende has X_{Mg} of 0.63–0.65. Ubiquitous ≤0.2 mm ilmenite shows hematite and pyrophanite contents of ≤5 mol% and 2–10 mol%, respectively.

[29] Medium-grained, mostly unfoliated, granular leucosomes (Figure S2q) comprise plagioclase, K-feldspar, quartz, and accessory zircon and apatite; some contain anhedral garnet or randomly oriented biotite. Plagioclase, K-feldspar, and garnet compositions are almost identical to adjacent melanosomes (e.g., 76175A, Tables S3 and S7), implying equilibration.

3.2.2. Fabrics and Mineral Composition of Intercalated Metabasites

[30] Medium-grained, layered metabasites of the central and southern Qinling complex contain amphibole, plagioclase, quartz, garnet, biotite, accessory ilmenite, apatite, and zircon, and secondary muscovite and epidote (Figure S2r). Euhedral garnet in 76163F has prograde zoning, with $Alm_{58}Grs_{19\text{-}20}Prp_{16}Sps_{6\text{-}7}$ in the core and $Alm_{62}Grs_{17}Prp_{17}Sps_4$ near the rim (Figure 8 and Table S3), and a retrograde pyrope decrease in the outermost rims. Other anhedral and poikiloblastic garnets have low spessartine (4–6 mol%), variable pyrope (8–18 mol%), and constant grossular (16–20 mol%) and almandine (64–68 mol%) contents; again, outermost rims have decreasing pyrope and increasing almandine and spessartine contents presumed to reflect retrogression. Weakly zoned amphiboles, with rimward increasing X_{Mg} and decreasing Ti, are tschermakite, ferrotschermakite, ferrohornblende, or magnesiohornblende; intersample variation shows X_{Mg} of 0.42–0.58, Si contents of 6.45–6.80 p.f.u., and Ti contents of 0.08–0.17 p.f.u (Table S6). Plagioclase has anorthite contents of 87–91 mol%. Biotite shows X_{Mg} values of 0.46–0.53 and Ti contents of 0.06–0.09 p.f.u. Ilmenite has ≤3 mol% hematite and 1–10 mol% pyrophanite contents.

3.2.3. Phase Equilibria and Metamorphic Conditions

[31] We performed equilibrium-assemblage calculations in the NCKFMASHT system with excess H_2O using bulk-rock compositions derived by point counting (Figures 9 and S5–S16). Partial melting of felsic gneisses started at 660–700°C at medium P; the lack of orthopyroxene and cordierite indicates a minimum P of 0.5–0.6 GPa and the ubiquitous sillimanite a maximum P of ~0.7–0.9 GPa. Garnet-core isopleth thermobarometry, thought to record peak P-T, refines these estimates. The westernmost sample (garnet-sillimanite gneiss Q33B, Figures 2 and S5) yielded ~743°C, 0.71 GPa. Farther east, felsic gneisses 75247F ~699°C, 0.66 GPa (Figures 2 and S6); 75248C ~693°C, 0.72 GPa (Figure S7); 75251E ~722°C, 0.62 GPa (Figure S8); and 76172C ~754°C, 0.75 GPa (Figure S9) yielded similar conditions. Farther south, garnet gneiss 76175A gave ~727°C, 0.52 GPa (Figures 2 and S10) and garnet-cummingtonite gneiss 75254A ~732°C, 0.75 GPa (Figure S11). Farther east, garnet gneiss 76163B yielded ~712°C, 0.61 GPa (Figure S12) and metabasite 76163 F, from the same outcrop, records garnet growth from ~675°C, 0.73 GPa to ~760°C, 0.68 GPa (Figure S13). Garnet gneiss 75271B, just west of the Songshugou complex (Figure 2), yielded ~702°C, 0.68 GPa (Figure S14). Garnet gneiss 811102F (northeastern central Qinling complex) provided the highest T, ~773°C, 0.51 GPa (Figure S15).

[32] Altogether, the intersections of almandine, grossular, and pyrope isopleths of garnet cores highlight upper amphibolite-facies metamorphism in the middle crust. The retrograde garnet rims preclude application of the isopleth method, as retrograde equilibration of Ca, Mg, and Fe with matrix phases might have stopped at different T. An exception is garnet gneiss 811079A (Figure S16): garnet-core isopleths yielded ~700°C, 0.80 GPa; similar to nearby samples, garnet rims point to ~680°C at 1.05 GPa. Here the isopleth method is applicable, as the calculated amount of garnet implies growth along the derived P-T path; these conditions coincide with the occurrence of kyanite in this area [*You et al*., 1993], and although at distinctly lower T, they resemble anticlockwise P-T paths recorded in granulites

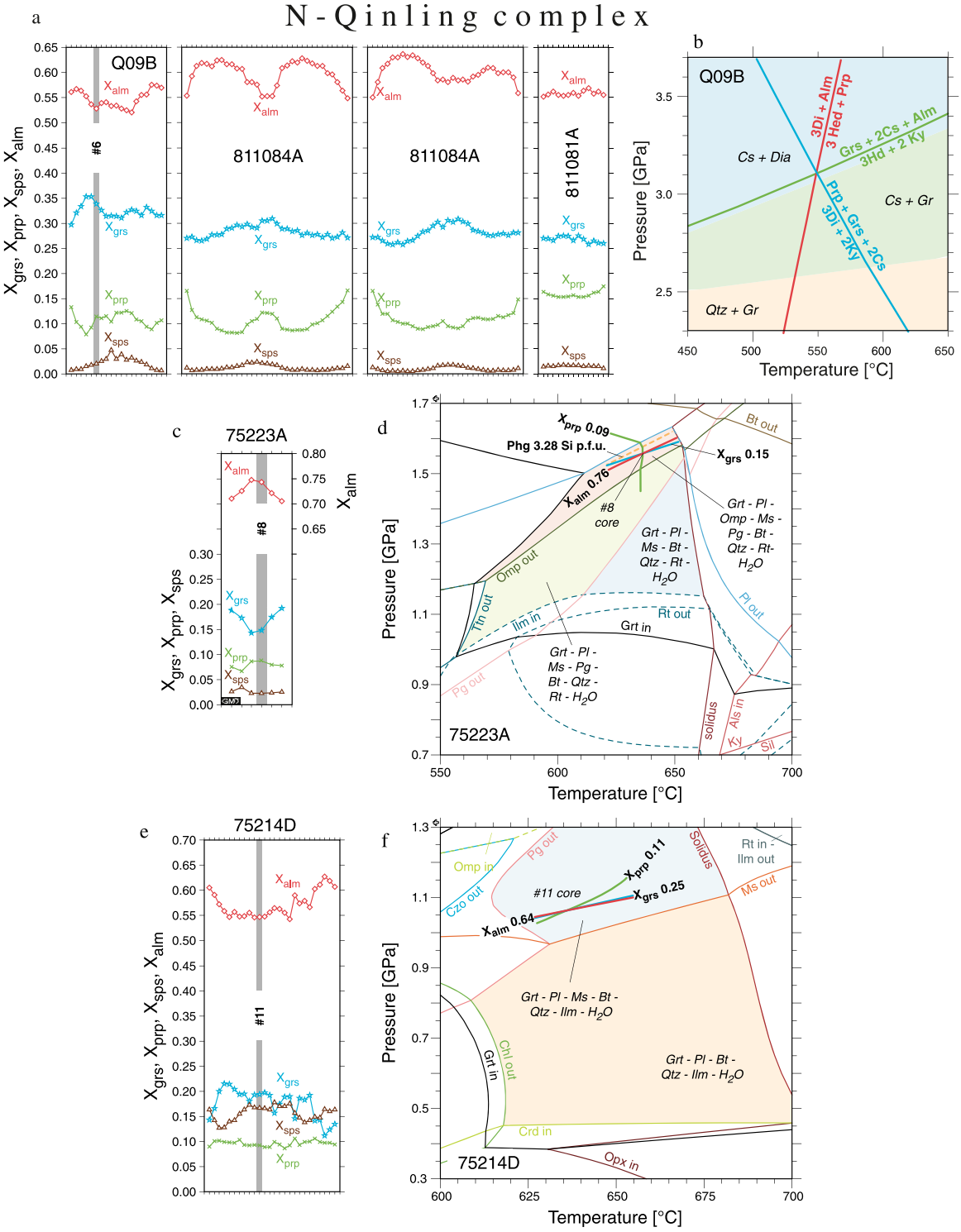

Figure 7. (a) Representative EMP profiles through garnet crystals from eclogites from the North-Qinling complex. Spacing of the microprobe spots is 20 µm. (b) Results of winTWQ multiequilibrium calculations applied to sample Q09B. (c) Representative EMP profile through a garnet from sample 75223A. The highlighted analysis corresponds to the isopleth intersection in Figure 7d. Spacing of microprobe spots is 10 µm. (d) Equilibrium-assemblage diagram (NCKFMASHT system, excess H_2O) and intersection of garnet-core isopleths of sample 75223A. Bulk-rock composition (in mol) is Si 24.176, Ti 0.179, Al 7.388, Fe 0.987, Mg 0.545, Ca, 0.179, Na, 1.324, K, 2.036, and O 63.183. (e) Representative EMP profile through a garnet from sample 75214D. The highlighted analysis corresponds to the isopleth intersection in Figure 7f. Spacing of microprobe spots is 20 µm. (f) As in Figure 7d but of sample 75214D. Bulk-rock composition (in mol) is Si 26.272, Ti 0.127, Al 4.528, Fe 1.071, Mg 0.955, Ca 0.743, Na 1.889, K 0.702, and O 63.6545. Mineral abbreviations follow *Kretz* [1983] and *Spear* [1993].

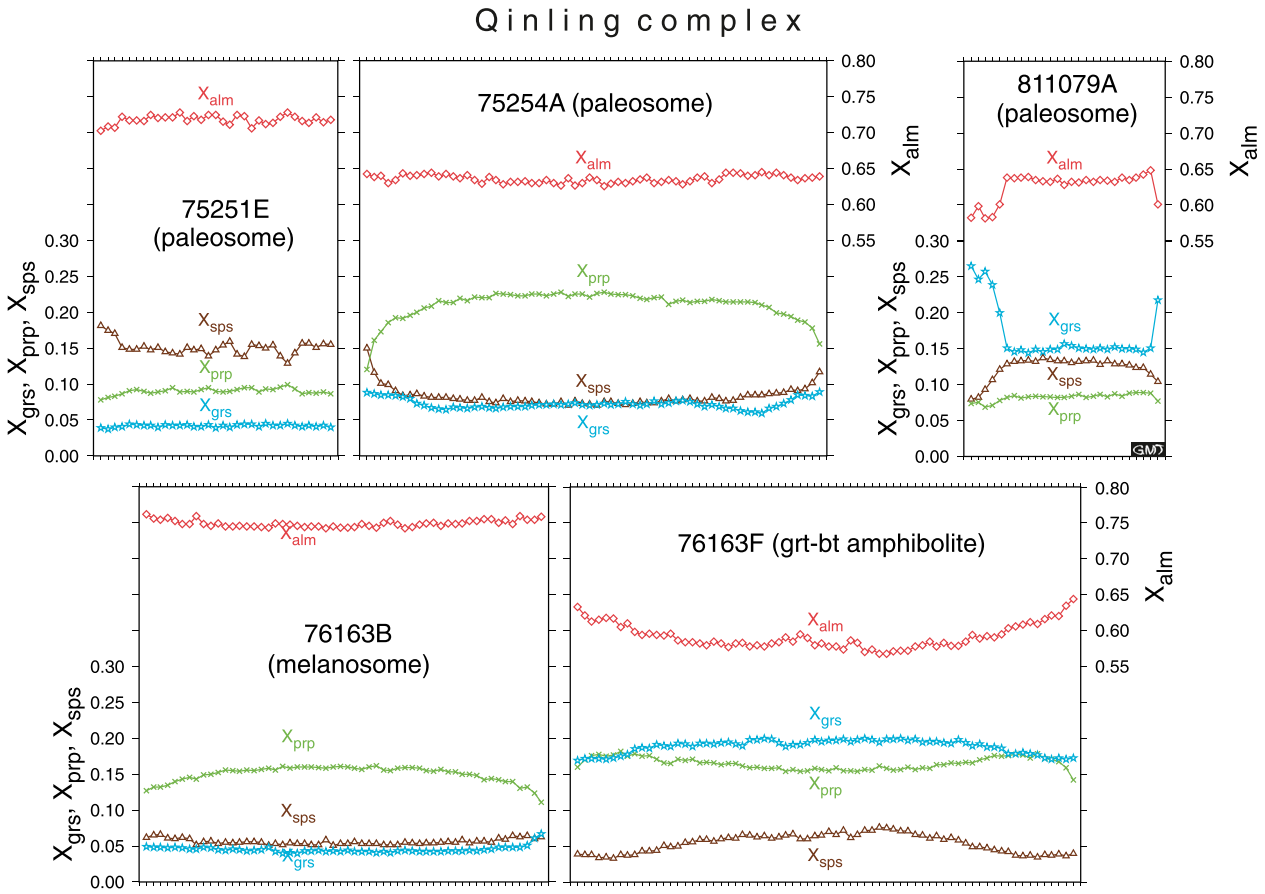

Figure 8. Representative EMP profiles through garnets from the Qinling complex. Spacing of microprobe spots is 20 μm.

from the Tongbai Shan [*Liu et al*., 2011; *Xiang et al*., 2012; *Bader et al*., 2012a].

3.3. Songshugou Ultramafic and Mafic Rocks: Petrography and Phase Equilibria

[33] The core of the Songshugou complex (Figure 2) contains granular, fine- to medium-grained, slightly altered spinel dunite to spinel lherzolite [cf. *Zhang*, 1999] with veins of coarse-grained olivine-websterite and olivine-clinopyroxenite (Figures S2s–S2v). Hydrous phases are cummingtonite, tremolite, phlogopite, and talc; retrograde serpentine occurs along grain boundaries and cracks. Spinel dunite 75295A from the center of the complex comprises a fine-grained matrix of olivine, euhedral amphibole, and accessory spinel (Figure S2s). Olivine has a X_{Mg} value of 0.90 (Table S9). Spinel is magnesiochromite with cores of $(Mg_{0.37}Fe^{2+}_{0.62})(Al_{0.29}Cr_{0.63}Fe^{3+}_{0.08})_2O_4$ and rims of $(Mg_{0.25}Fe^{2+}_{0.74})(Al_{0.15}Cr_{0.65}Fe^{3+}_{0.19})_2O_4$ (Table S10). Amphibole has tremolite cores ($X_{Mg}=0.96$) and cummingtonite rims ($X_{Mg}=0.87$; Figure 10a and Table S6). Phase-equilibrium calculations in the CKFMASH system with excess H_2O yielded a stability field at 650–710°C, <0.8 GPa for the assemblage tremolite-cummingtonite-olivine-spinel (Figure 10b); these P-T conditions were achieved during the incorporation of the upper mantle peridotite into the crust. Olivine-spinel thermometry [*Ballhaus et al*., 1991; *O'Neill and Wall*, 1987] yielded 600–630°C at the above P; this may record retrograde cooling.

[34] Meter-sized spinel-peridotite boudin 75257A, in contact with migmatite, is the southernmost sample of the gneiss-amphibolite-migmatite association we investigated in the western East-Qinling complex (Figure 2); we attribute this rock to the southerly abutting Danfeng complex and correlate it with the Songshugou ultramafic rocks farther east. The spinel peridotite has primary olivine, orthopyroxene, and spinel and secondary amphibole and phlogopite in a serpentine matrix (Figures S2u and S2v). Olivine and orthopyroxene show X_{Mg} values of 0.89–0.90, and magnesiochromite has cores of $(Mg_{0.34}Fe^{2+}_{0.65})(Al_{0.26}Cr_{0.69}Fe^{3+}_{0.05})_2O_4$ and rims of $(Mg_{0.28}Fe^{2+}_{0.71})(Al_{0.15}Cr_{0.81}Fe^{3+}_{0.04})_2O_4$. Amphibole prisms have tremolite cores ($X_{Mg}=0.96$) and cummingtonite rims ($X_{Mg}=0.87$); needles are unzoned cummingtonite (Figure 10a and Table S6). Phlogopite has colorless cores ($X_{Mg}=0.95$) and bluish rims with a slightly higher Fe content ($X_{Mg}=0.92$; Table S8 and Figures S2u and S2v). During exhumation from mantle depths, sample 75257A experienced hydrous metasomatism with growth of tremolite at the expense of primary clinopyroxene. Subsequently, cummingtonite formed at the expense of orthopyroxene. The equilibrium assemblage tremolite-cummingtonite-orthopyroxene-olivine-phlogopite is stable in a narrow field at 680–740°C, <1.1 GPa (Figure 10c). Olivine-spinel thermometry [*Ballhaus et al*., 1991] yielded 630–700°C for an assumed P of 1 GPa.

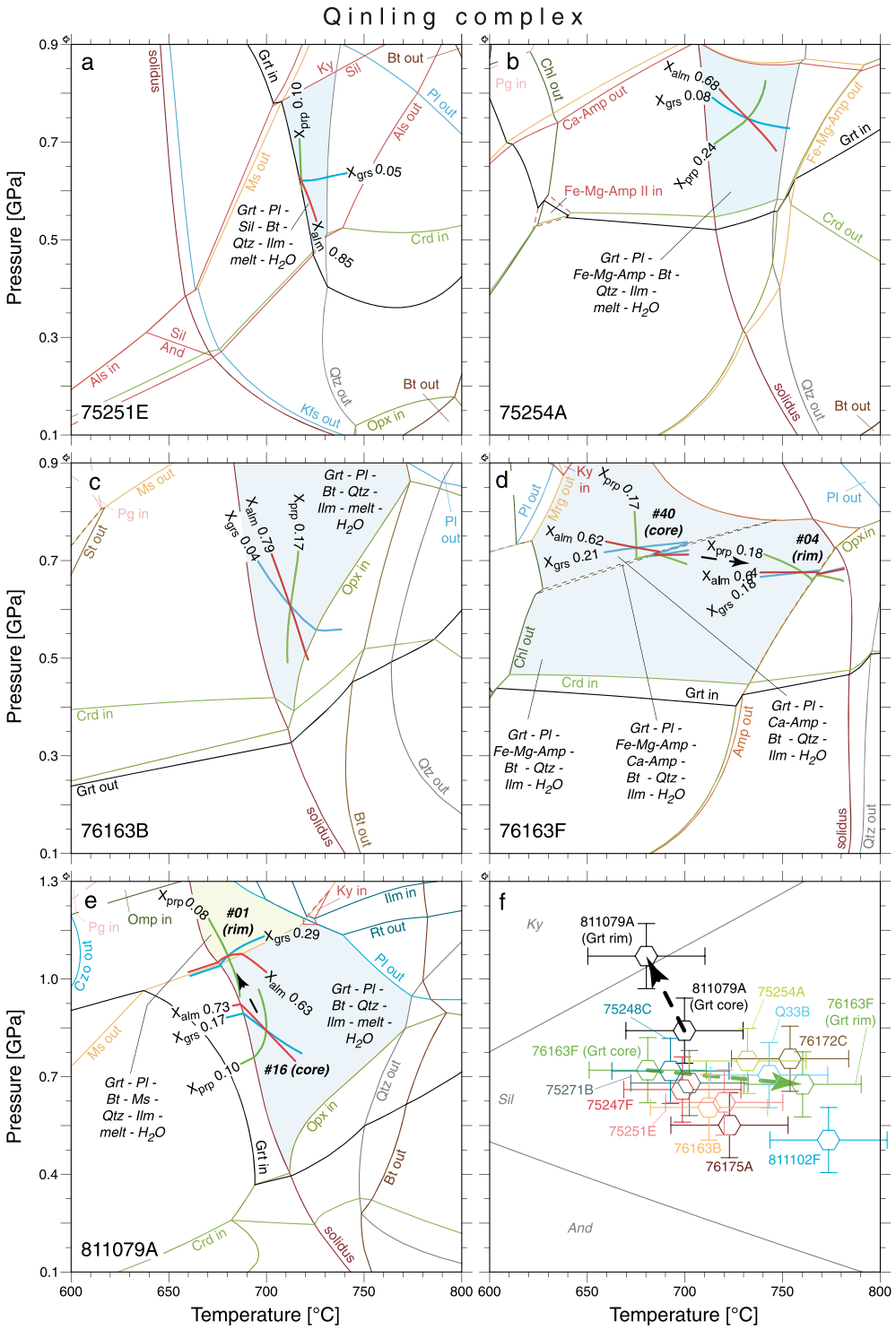

Figure 9. Results of equilibrium-assemblage calculations (NCKFMASHT system, excess H_2O) applied to gneisses of the Qinling complex. The bulk-rock compositions were obtained by point counting. (a) Garnet-bearing sillimanite gneiss (melanosome) 75251E. The bulk-rock composition (in mol) is Si 23.379, Ti 0.399, Al 6.745, Fe 1.887, Mg 0.582, Ca 0.667, Na 1.580, K 2.084, and O 62.6415. (b) Garnet-cummingtonite gneiss (melanosome) 75254A. The bulk-rock composition (in mol) is Si 20.373, Ti 0.233, Al 6.573, Fe 2.207, Mg 2.212, Ca 1.364, Na 1.977, K 1.000, and O 58.343. (c) Garnet gneiss (blastomylonite; melanosome) 76163B. The bulk-rock composition (in mol) is Si 24.300, Ti 0.221, Al 5.741, Fe 1.871, Mg 0.957, Ca 0.923, Na 2.116, K 0.866, and O 62.8955. (d) Garnet amphibolite 76163 F. The bulk-rock composition (in mol) is Si 19.345, Ti 0.693, Al 6.613, Fe 5.194, Mg 3.594, Ca 1.603, Na 0.166, K 1.548, and O 61.2435. (e) Garnet gneiss (melanosome) 811079A. The bulk-rock composition (in mol) is Si 23.287, Ti 0.209, Al 6.069, Fe 1.800, Mg 0.970, Ca 1.176, Na 2.168, K 1.016, and O 61.6335. (f) Summary of obtained P-T data.

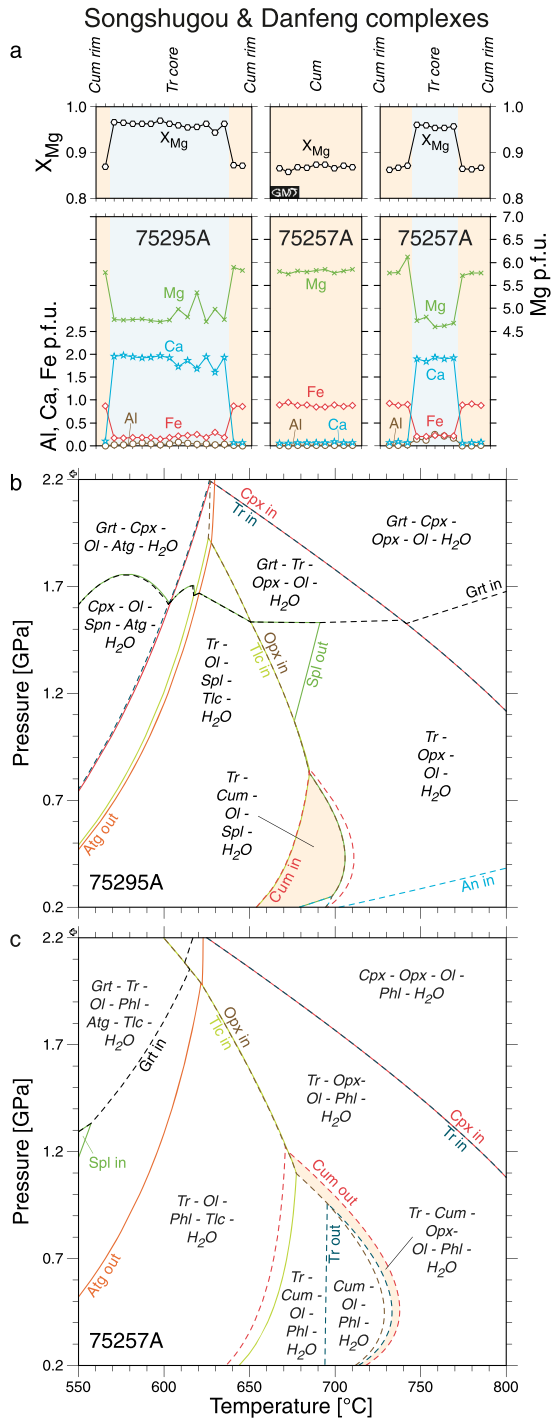

Figure 10. (a) EMP profiles across amphibole crystals from ultramafites 75295A (Songshugou complex) and 75257A (Danfeng complex). (b) Equilibrium assemblage diagram of sample 75295A. The bulk-rock composition (in mol) obtained via XRF analysis is Si 14.709, Al 0.133, Fe 2.444, Mg 24.498, Ca 0.177, and O 56.7365. (c) Equilibrium assemblage diagram of sample 75257A. The bulk-rock composition (in mol) obtained via XRF analysis is Si 16.731, Al 0.305, Fe 2.381, Mg 21.163, Ca 0.222, K 0.158, and O 57.7645. To overcome destabilization of spinel by exclusion of Cr from the calculations due to the lack of thermodynamic data, Al-rich phases chlorite, cordierite, and chloritoid were excluded from the calculation of both diagrams.

[35] The metabasites of the Songshugou complex record a HP evolution prior to a widespread medium-P, upper amphibolite-facies overprint. Based on garnet zoning and thermodynamic modeling, *Bader et al.* [2012b] calculated a prograde P-T path, ~498°C, 2.25 GPa to ~530°C, 2.54 GPa, from garnet amphibolite 75293E. Conventional thermobarometry [*Colombi*, 1988; *Bhadra and Bhattacharya*, 2007] applied on clinoamphibole-plagioclase-quartz coronas around garnet constrained subsequent heating to 660–700°C, 1.1–1.2 GPa, which is much colder than that envisioned for the mafic HP granulites studied by *Zhang* [1999].

3.4. Geochronology

3.4.1. Erlangping Complex

[36] We analyzed diorite Q10 of the "mafic" rock sequence and syenite Q125 intruding this sequence (Tables S2 and S11, and Figures 2 and 4b) to better constrain the age range of Erlangping-complex magmatism. Magmatic zircons (Th/U = 0.2–0.9, mean = 0.5; oscillatory zoning in cathodoluminescence (CL)) of the diorite crystallized at 487.1 ± 6.4 Ma; they show no inheritance. This is the oldest reported crystallization age for the Erlangping complex. The syenite crystallized at 418.6 ± 6.6 Ma (magmatic zircons, Th/U = 0.4–2.6, mean = 1.0; oscillatory zoning), with older Paleozoic inheritance. Figure 4c combines our new ages with the published ages; the transition from "more mafic to more felsic" rocks may reflect an evolution from "intraoceanic/back-arc" to "continental margin" arc magmatism.

3.4.2. North-Qinling Complex

[37] Our geochronology aimed to provide a minimum age for the UHP metamorphism. Titanite grew from rutile (≤650°C retrograde overprint of section 3.1) at 471 +17/−16 Ma (U-Pb titanite, garnet amphibolite 811084) and ^{40}Ar-^{39}Ar phengite records cooling through ~400°C at 470 ± 1 Ma (paragneiss 75223A; Tables S2 and S11 and Figure 5g).

3.4.3. Qinling Complex

[38] We aimed to elucidate the age of magmatism in the UM section and to reveal relationships among the mafic and felsic rocks along N-S transects across the western East-Qinling. Concordant zircons in garnet-sillimanite gneiss Q33, an isoclinally folded melanosome, span 537–368 Ma. A dominant group at 502.4 ± 5.9 Ma and younger—up to Devonian—magmatic zircons (Th/U = 0.4–1.9, mean = 1.0; oscillatory zoning; Figure 5 h) may indicate prolonged magmatic activity. Along the gorge of the Weihe River in the western Qin Mountains, Qinling-complex granodiorite Q123 underlies Erlangping-complex rocks. Zircons in the granodiorite crystallized at 473.2 ± 6.8 Ma (Th/U = 0.2–0.6, mean = 0.43; oscillatory zoning) and lack inheritance (Figure 5 h).

[39] A N-S profile along the southern border of the 438 ± 3 Ma Huichizi pluton [*Li et al.*, 2000; *Wang et al.*, 2009; *Bader et al.*, 2013] addresses migmatization and high-grade mylonitization. Leucogranite mylonite 76162H has a group of matrix monazites at 397.1 ± 5.4 Ma (Th-Pb SIMS age, Figure 5i), likely recording recrystallization during HT mylonitization; myrmekite is ubiquitous and quartz recrystallized by grain-boundary migration. A continuum of progressively younger ages down to ~352 Ma suggests a thermal overprint or continued recrystallization. The zircons in the melanosome of garnet-hornblende-biotite schist

76163F are metamorphic (mean Th/U = 0.07; well-rounded, structureless grains in CL; Figures 5i and S17a) and span ~505–398 Ma; migmatization occurred at 464.0 ± 2.9 Ma, indicating a HT event prior to the peak of regional magmatism (~425 Ma, section 2.4). Blastomylonitic garnet gneiss 76163B of the same outcrop, also a melanosome, yielded a 380.5 ± 7.4 Ma Th-Pb SIMS matrix-monazite age, close to the youngest zircon in the schist (Figure 5i). Again, a continuous series of progressively younger ages suggests thermal overprint, likely represented by a group of monazites at 351.9 ± 5.9 Ma; this is consistent with sample 76162H above.

[40] Orthogneisses dominate our N-S profile across the western East-Qinling (Figures 2 and 5j), with paragneiss melanosome and amphibolite with boudin necks filled with syntectonic pegmatitic gneiss (leucosome). Grey orthogneiss 75246A has many discordant zircons; although apparently magmatic (Th/U = 0.004–0.36, mean = 0.21), nearly all zircons show uniform CL, indicative of HT homogenization or recrystallization (Figure S17b). Concordant grains span 547–353 Ma. The gneiss likely crystallized at 450.6 ± 3.1 Ma (concordia age, identical with lower intercept age, Figure 5j). The youngest concordant zircon at ~353 Ma corresponds to a lower intercept age of ~351 Ma. Postmigmatitic granite 75244C yielded a 394.9 ± 3.3 Ma Th-Pb SIMS monazite age. Concordant, mostly magmatic zircons (Th/U = 0.09–2.04, mean = 0.6) of amphibolite 75247C span 620–388 Ma; two groups with similar Th/U ratios (0.52 and 0.76) and CL appearance (patchy to oscillatory to uniformly dark zoning, Figure S17c; 435.2 ± 6.5 and 401.7 ± 4.3 Ma) are younger than high-U zircons at ~567 Ma (bright CL appearance in Figure S17c; Figure 5j). The two age groups are identical to those of pegmatite 75247D in the necks of the 75247C amphibolite boudins: 435.5 ± 2.5 and 400.6 ± 3.1 Ma. The younger age group comprises zircons with lower Th/U (0.09–0.57, mean = 0.25) than the older group (Th/U = 0.19–1.30, mean = 0.50) and includes grain rims and small grains (Figure S17d). A few older magmatic zircons are at 475.7 ± 5.7 Ma.

[41] The southern part of our western East-Qinling profile (Figures 2 and 5k) is dominated by granitoids and shows intercalations of amphibolite and gneiss; these typically migmatitic rocks extend to a section dominated by meta(ultra)mafic rocks, classified as part of the Danfeng complex. Two garnet amphibolites (75255A and 75256A) are locally associated with ultramafic rocks and are inclusions in orthogneiss. Concordant zircons in 75255A span 1439–501 Ma, but every grain except the youngest is Neoproterozoic [Bader et al., 2013]. In 75256A, the oldest grain is ~728 Ma and the other zircons may comprise three age groups, 456.2 ± 7.8, 486.7 ± 4.7, and 514.8 ± 7.3 Ma, that all have low Th/U ratios (mean = 0.13) and patchy CL appearance, with rare blurred oscillatory zoning (Figure S17e). Penetratively foliated amphibolite (75251B) has a 404.6 ± 3.6 Ma U-Pb titanite age; it likely dates deformation. Coarse-grained, postmigmatitic syenogranite 76173A, with myrmekite and dynamically recrystallized quartz, has a 392.4 ± 4.2 Ma Th-Pb monazite age. Granite 75253B likely crystallized at 386.6 ± 3.8 Ma (mean Th/U = 0.46, oscillatory zoning in all zircons) and has inherited age groups at 406.1 ± 3.0 and 442.4 ± 6.2 Ma; all these groups have zircons with CL growth zonation and mean Th/U ratios of ~0.4. Even younger ages (366.9 ± 7.8 Ma lower intercept of seven zircon spots, sample 75253B; ~354 Ma monazite, sample 76173A) correspond to those observed in the other profiles (see above). Garnet gneiss 76172C has two zircons at 487 ± 11 Ma besides mostly Neoproterozoic ages [*Bader et al*., 2013].

[42] Figure 5l summarizes our new data from the southern Qinling-complex profiles; we conclude that (1) reheating occurred at ~360 Ma (we will detail this event in part III of this paper series), (2) migmatization terminated at ~400 Ma, (3) synkinematic intrusion and HT mylonitization occurred at ~400 Ma (we will detail the deformation in part III of this paper series), (4) apparently continuous magmatism spans at least 515–400 Ma, and (5) there is no distinct crystallization event for the amphibolite protoliths.

3.4.4. Danfeng and Songshugou Complexes

[43] We aimed to substantiate the distinction between an early more mafic and a younger, more felsic rock group in the Danfeng complex (cf. Figure 6a) and to constrain the retrograde path of the Songshugou-complex rocks. Western Qinling greenschist Q122 yielded magmatic (e.g., Th/U = 0.1–0.7, mean 0.3; oscillatory zoning) zircon ages that span 2186–478 Ma (Figure 6d), indicating a tuffitic protolith. The igneous component likely crystallized at 499.4 ± 9.3 Ma; the detrital age groups at ~810, 960, and 1074 Ma are typical for the Neoproterozoic evolution of the Qinling orogenic collage [*Bader et al*., 2013]. Massive granodiorite Q31 crystallized at 433.3 ± 9.6 Ma (Th/U = 0.5–1.3, mean = 0.9; oscillatory zoning); it lacks inheritance (Figure 6d).

[44] Traditionally, felsic garnet gneiss melanosome 75271B and garnet amphibolite 75271A from the same outcrop would be classified as Qinling complex and Fushui-intrusive complex, respectively. 75271B Th-Pb matrix monazite ages yielded a continuous series of progressively younger ages, suggesting ≥459 Ma metamorphism overprinted by ~343 Ma reheating. 75271A garnet amphibolite contains relic rutile and ilmenite in titanite; the titanite formed at 324 ± 12 Ma, within error overlapping the monazite ages of 75271A. These are the youngest HT ages obtained so far.

4. Discussion

[45] To first order, the evolution of magmatism and metamorphism in the Qinling-Tongbai orogen took place in two stages (Figures 11 and 12). The age of magmatism and metamorphism is pre-~460 Ma in the Songshugou-Fushui and North-Qinling complexes and mostly pre-~460 Ma in the Danfeng complex; it is mostly post-~460 Ma in the Kuanping and Erlangping complexes, and the Qinling complex has both age components (Figure 11a). The North-Qinling, Qinling, and Songshugou complexes have (U)HP metamorphism; the Songshugou and Qinling complexes have HT, locally UM, the Erlangping and Kuanping complexes only in the Tongbai Shan (Figure 12). UHT metamorphism affected the Qinling complex in the Tongbai Shan. (U)HP metamorphism in the North-Qinling complex and the Qinling complex is ~497 and 490–473 Ma, respectively. Relatively high-P HT metamorphism (mafic HP granulites) is ~504 Ma in the Songshugou-Fushui complex (Figures 6c and 12b). Medium-P HT metamorphism is ~440–414 Ma in the Qinling, Erlangping, and Kuanping

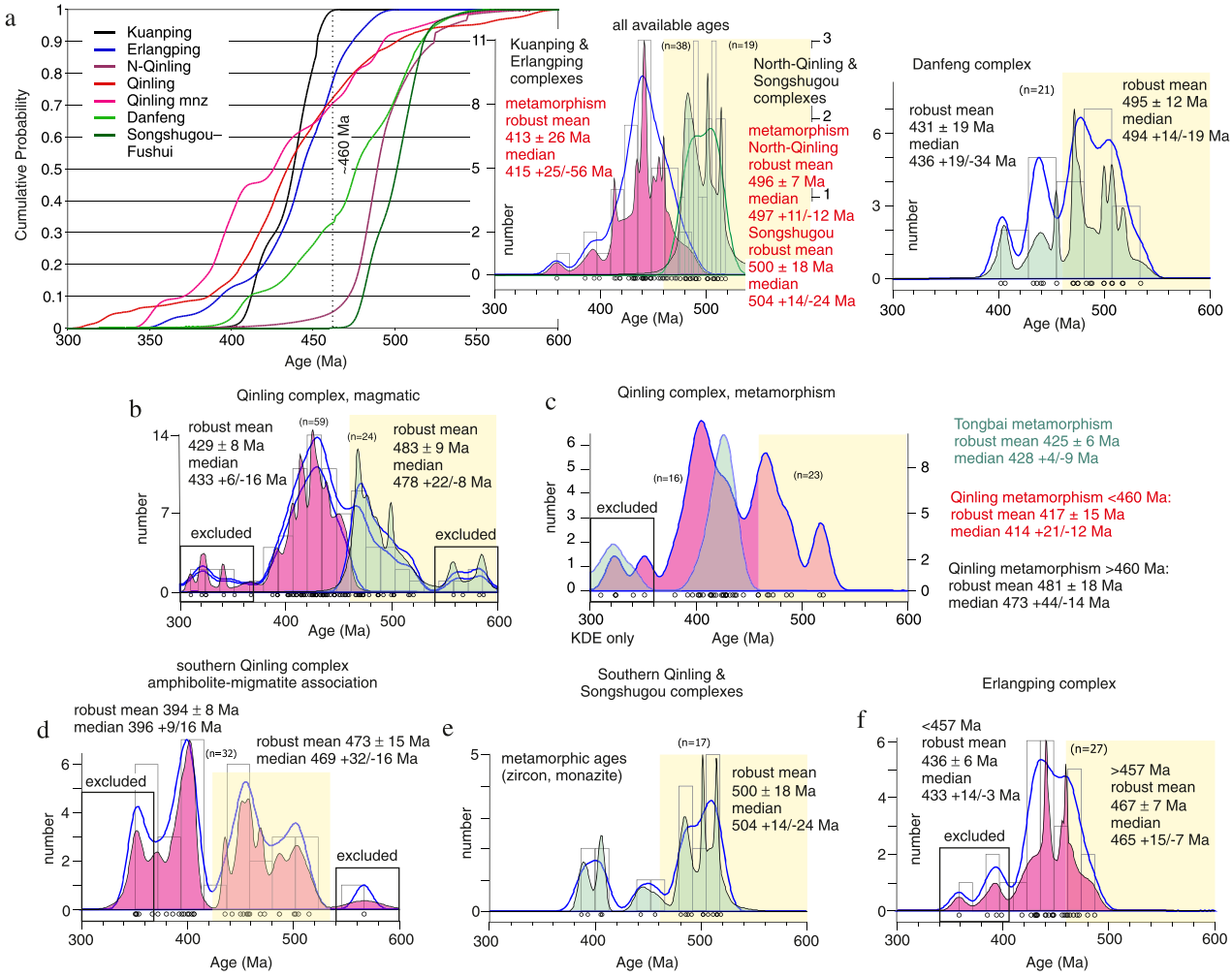

Figure 11. Summary of age data. (a) Cumulative probability plot comparing the U/Th-Pb ages from the various complexes of the Qinling orogenic collage. Mnz, monazite. Diagrams on the right, calculated with "*densityplotter*" [*Vermeesch*, 2012], emphasize specific data of some complexes and give robust means and medians (see Appendix A) for these data. Diagrams comprise kernel density estimates (blue line, calculated with a bandwidth of 8), probability density plots (reddish or greenish background), and histograms. Circles at bottom give the data distribution. (b–f) As in Figure 11a but for specific data of other complexes; "excluded" marks data not incorporated in the calculations of the robust means/medians. See text for discussion.

complexes of the Tongbai Shan (Figures 5b and 12), and metamorphic zircon and monazite in the Qinling complex of the Qinling have a major cluster at ~415 Ma. Thus, (U) HP metamorphism in the North-Qinling and Qinling complexes was about coeval with relatively high-P HT metamorphism (mafic HP granulites) in the Songshugou-Fushui complex; metamorphism in these complexes is distinctly older than the main body of HT (UM) metamorphism in the Qinling complex.

[46] In detail, the evolution of magmatism and metamorphism is more complex. Excluding the <370 Ma "reheating" ages (chapter 3.4.3) and four ages >540 Ma, the Qinling-complex age distribution is bimodal, with medians at ~478 and 433 Ma (Figure 11b). Metamorphic zircon and monazite ages alone show a similar, albeit less distinct, distribution (medians at ~473 and 414 Ma; Figure 11c). Our study of magmatism and UM in the gneiss-amphibolite-migmatite association in the southern Qinling complex also shows two broad groups of magmatic and metamorphic ages, separated by a gap between ~407 and 436 Ma (Figure 11d). In these profiles, we attempt to refine dating of metamorphism: Magmatic and metamorphic zircons, in particular in melanosome, trace continuous magmatism and related metamorphism through ~503–436 Ma (Figure 5l), overlapping with HT metamorphism in the Songshugou and northern Danfeng complexes. Assuming that the leucosomes and postmigmatitic, partly pegmatitic (leuco)granites formed during the last stage of UM, our samples date UM at ≥397 Ma (median, n = 6; Figure 5l). Zircons in garnet-sillimanite gneiss migmatite Q33 crystallized at ~502 Ma, but a tail of younger ages stretches into the Devonian; metamorphism (~743°C) cannot be assigned clearly to an age, but migmatization was likely as old as Middle Cambrian. Garnet-gneiss melanosome 76172C has mostly Neoproterozoic zircons but likely crystallized at ~487 Ma, suggesting an Early Ordovician peak metamorphism

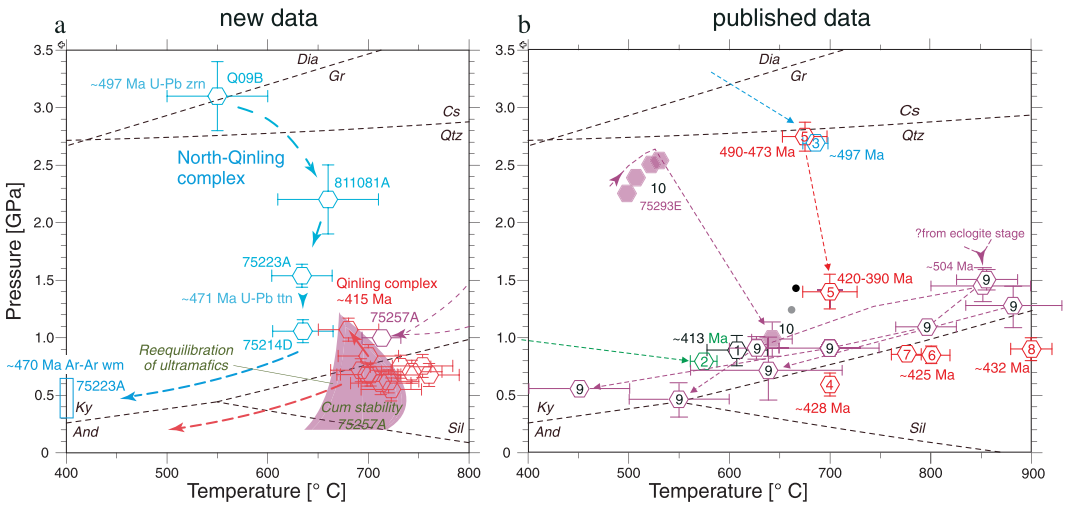

1, Kuanping, ~415 Ma metamorphism, Tongbai Shan [*Liu et al.*, 2011]
2, Erlangping, ~415 Ma metamorphism, Tongbai Shan [*Ratschbacher et al.*, 2006; *Liu et al.*, 2011]
3, North-Qinling, ~497 Ma HP-UHP metamorphism [*Yang et al.*, 2003; *Cheng et al.*, 2012]
4, Qinling complex, Qinling, (U)HT metamorphism [*You et al.*, 1993]
5, Qinling complex, Qinling, 490-473 Ma, HP metamorphism [*Cheng et al.*, 2011]
6, Qinling complex, Tongbai Shan, ~428 Ma HT metamorphism [*Liu et al.*, 2011]
7, Qinling complex, Tongbai Shan, HT metamorphism [*Bader et al.*, 2012a]
8, Qinling complex, Tongbai Shan, UHT metamorphism [*Xiang et al.*, 2012]
9, Songshugou complex, ~504 Ma peak metamorphism and later retrograde overprint [*Liu et al.*, 1995, 1996; *Zhang*, 1999]
10, Songshugou-complex meta-basite, HP to HT metamorphism [*Bader et al.*, 2012b]

Figure 12. Summary of (a) new and (b) published pressure-temperature data. Age assignment of specific data or P-T spaces from data sources discussed in the text. Cum, cummingtonite; ttn, titanite; zrn, zircon; wm, phengite.

(~754°C). Garnet-hornblende-biotite schist 76136F (melanosome) records decompressional heating (~675 to 760°C; 0.73 to 0.68 GPa), and garnet gneiss 76163B (melanosome) of the same outcrop shows peak T at ~712°C; metamorphic zircons in 76136F and monazite in 76163B bracket this P-T evolution between ~464 and 381 Ma. As we interpret most of the gneiss-amphibolite-migmatite association as a strongly overprinted section of the Songshugou-Fushui complex, a combination of the metamorphic ages from these units may best characterize the duration of HT metamorphism: there is continuous metamorphic activity with peaks at ~500 and 400 Ma (Figure 11e).

[47] The age distribution in the Danfeng complex (Figure 11a) may also be interpreted as reflecting two age groups; as stated earlier, these may reflect formation of mostly basites during the Late Cambrian (median at ~494 Ma) and of mostly andesites during the Silurian (median at ~436 Ma). Geodynamically, these age groups may record oceanic spreading and arc magmatism; we correlate the latter (median at ~436 Ma) with the younger period of magmatism and HT (UM) metamorphism in the Qinling complex (median at ~433 Ma). The ages of the Erlangping complex may be interpreted accordingly (Figure 11f); the older ages (median at ~465 Ma), of more mafic rocks, trace oceanic spreading, and the younger ages (median at ~433 Ma), of more felsic rocks, arc magmatism that is the same as in the Qinling complex. It is a cornerstone of the Qinling-Tongbai orogen evolution that the Silurian–Early Devonian arc magmatism straddles the boundaries of the Danfeng, Qinling, Erlangping, and Kuanping units (Figure 2) [e.g., *Ratschbacher et al.*, 2003]; this is supported by our analysis.

[48] We conclude that the North-Qinling, Qinling, and possibly, Songshugou complexes may have a ~500 Ma (U) HP evolution; the age of the low-T HP evolution (~498°C, 2.25 GPa to ~530°C, 2.54 GPa) [*Bader et al.*, 2012b] in the Songshugou garnet amphibolite is unknown but certainly older than the ~420 Ma UM in the Qinling complex. This (U)HP metamorphism represents P-T-t snapshots along different parts of a wide subduction-accretion system that involved a crustal wedge, the Meso-Neoproterozoic core of the Qinling complex; this subduction-accretion system comprised a "Grenville" oceanic-clastic wedge to its north (North-Qinling unit) [*Bader et al.*, 2013] and a wedge with ultramafic-mafic-felsic igneous and clastic rocks in the south (eclogite of *Cheng et al.* [2011]) transitional into our gneiss–amphibolite-migmatite association that includes a southern mantle wedge, the Songshugou ultramafic rocks and equivalents in the Danfeng complex. This subduction-accretion system was active contemporaneously with a first period of magmatism and HT metamorphism (our pre-~460 Ma event). After a decrease in magmatism and metamorphism, this subduction-accretion system, the adjacent oceanic systems (Danfeng and Erlangping complexes), and the clastic unit of the Kuanping complex were involved in a second period of magmatism and HT metamorphism (our post-~460 Ma event) that peaked with regional UM at ~420–400 Ma.

[49] In the following, we present a tectonic model that integrates the (U)HP and (U)HT/UM evolutions and discuss this model using the tectonostratigraphic, metamorphic, and geochronologic data derived from the various complexes in the Qinling-Tongbai orogen. Figure 13 summarizes the key data

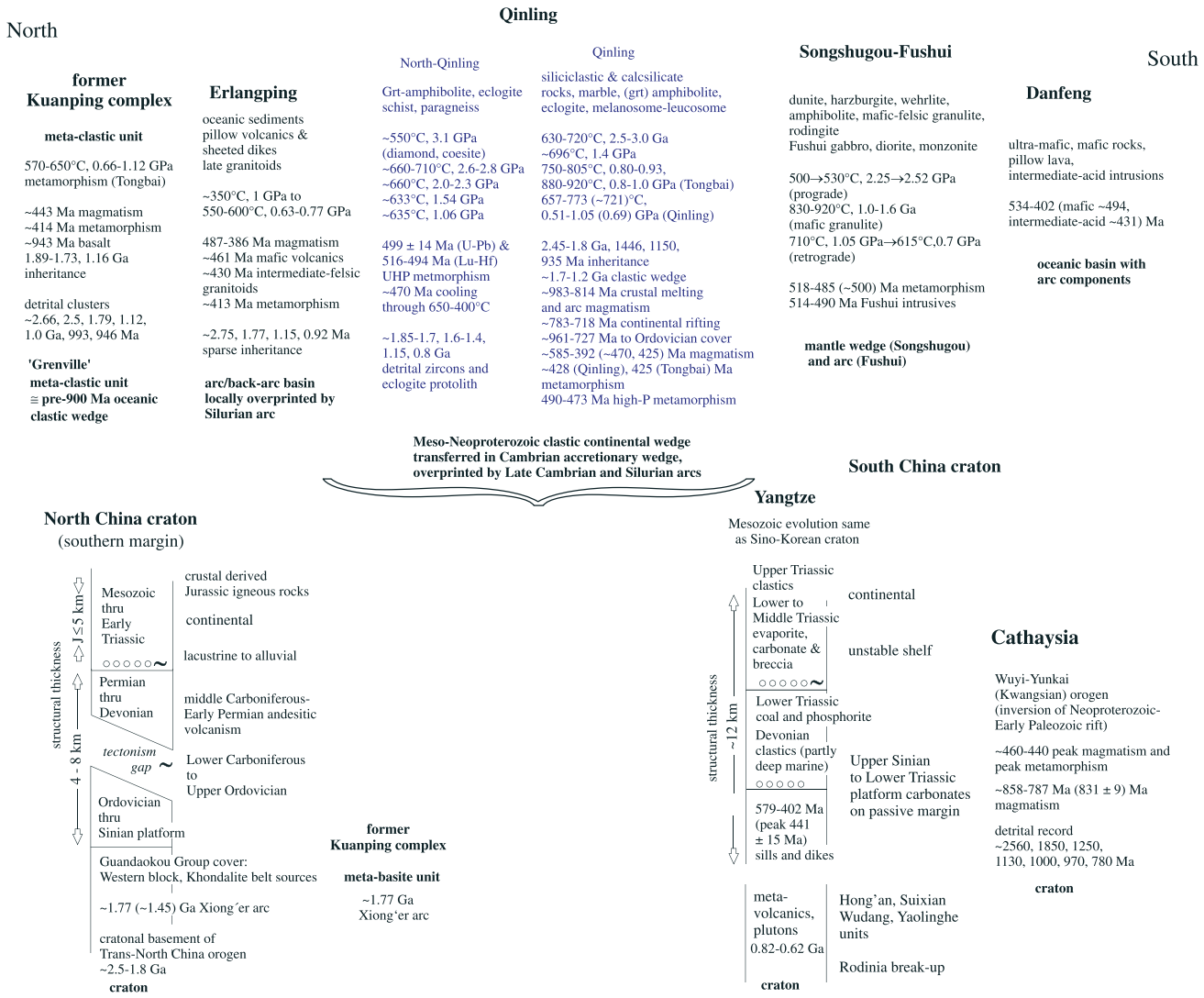

Figure 13. Summary of the tectonostratigraphy, pressure-temperature-time data, and tectonic interpretation of the complexes of the Qinling orogenic collage.

from the entire Qinling orogenic collage, and Figures 14a and 14b illustrate our tectonic model in two time slices: pre- and post-~460 Ma; it also attempts an along-strike correlation with the Qilian orogen in the west (Figure 14c). Figures 14d and 14e summarize the two major previous geodynamic interpretations of the Qinling-Tongbai collage [*Ratschbacher et al*., 2003; *Dong et al*., 2011a] for comparison. The core of the new model is the concentration of subduction-accretion along the margins of the Precambrian Qinling-complex crustal core and the subduction of relatively young lithosphere and ultimately of a spreading ridge that provided the heat to generate (U)HT/UM metamorphism.

[50] Postsupercontinent Rodinia rifting and oceanic spreading established wide ocean basins ("Neoproterozoic-Cambrian ocean basin," Figure 14a) north and south (in present coordinates) of the Qinling complex, i.e., between the NCC, the Qinling complex, and the SCC [e.g., *Li et al*., 2008a]. Subduction, likely intraoceanic, nucleated in the Early Cambrian within the oceanic domain north of the Qinling complex, ultimately forming the North-Qinling complex subduction-accretion wedge. Remnants of Neoproterozoic oceanic lithosphere may be preserved as the ~0.8 Ga protolith of North-Qinling complex eclogite. It is likely that this subduction-accretionary system developed close to the Qinling complex, given the comparable Paleo-Mesoproterozoic detrital and inheritance zircon record of the North-Qinling and Qinling complexes [*Bader et al*., 2013]. We associate the Erlangping complex with this subduction system, constituting an intraoceanic arc–back-arc system [*Xue et al*., 1996; *Dong et al*., 2011a]; this subduction-accretion system would be relatively short lived given the age range of its early, "oceanic" magmatic period (~490–450 Ma, Erlangping-complex intraoceanic arc–back arc; Figure 4c) and the exhumation of the UHP rocks (both eclogite and paragneiss) to crustal depths at ~470 Ma in the North-Qinling complex subduction-accretion wedge (Figure 12a).

[51] We suggest that up to three subduction zones were present south of the Meso-Neoproterozoic core of the Qinling complex (as sketched in Figure 14a). However, scenarios with less, perhaps oppositely dipping zones, or even one subduction zone that may have jumped in time or involved wholesale subduction of the Qinling complex, would

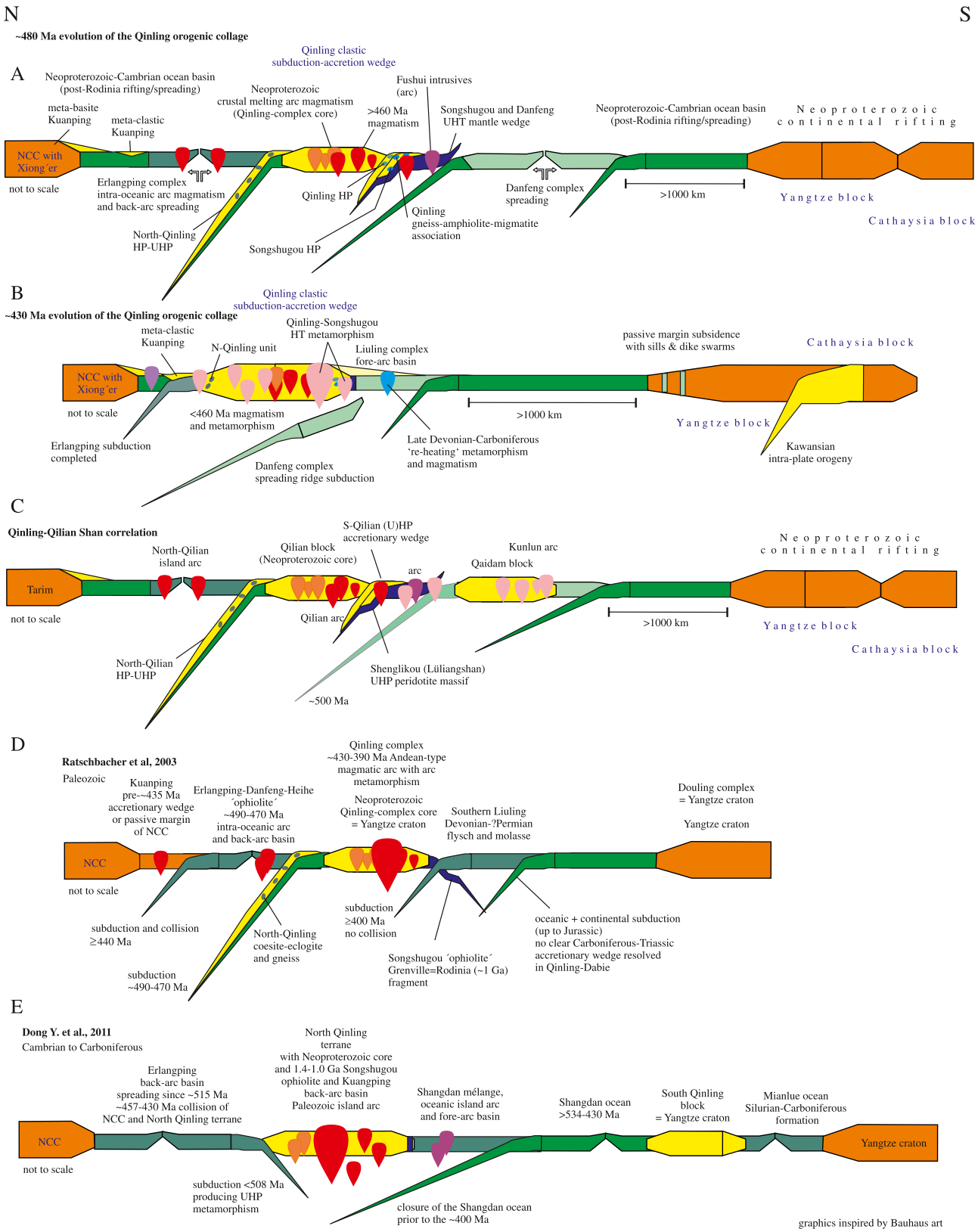

Figure 14. (a–e) Schematic, not-to-scale cartoons of Cambrian-Devonian evolution of the Qinling orogenic collage and (c) an attempt of a correlation with the Qilian Shan orogenic collage >500 km to the west. (d and e) The two major previous geodynamic interpretations of the Qinling-Tongbai collage [*Ratschbacher et al*., 2003; *Dong et al*., 2011a] summarized for comparison.

also account for the subduction-process snapshots currently understood; these snapshots comprise incompletely conserved, apparently distinct HP-UHP metamorphic histories, i.e., diamond-field UHP metamorphism in the North-Qinling complex, relatively high-T, nearly UHP metamorphism in the central Qinling complex, and relatively cold HP metamorphism and HT metamorphism that possibly evolved out of a eclogite-facies stage (mafic HP granulites) in the Songshugou complex (Figure 13). In our preferred scenario, we suggest that another subduction zone–besides the North-Qinling complex one–nucleated along the only continental sliver that is known between the NCC and SCC, the Qinling-complex crustal wedge; this would account for the preferred initiation of subduction along rheologic heterogeneities in the lithosphere. We place this subduction zone south of the Qinling-complex core; it formed the Qinling-complex HP eclogite [*Cheng et al*., 2011] during the Late Cambrian. The subduction process accreted rocks derived from the Qinling-complex core to the north (e.g., Neoproterozoic garnet gneiss 76172C) and possibly remnants of Neoproterozoic oceanic lithosphere, e.g., the ~899 Ma garnet amphibolite in the southern Qinling complex [*Bader et al*., 2013] into the wedge. This subduction zone may also account for the relatively cold HP metamorphism in the Songshugou garnet amphibolite (10 in Figure 12b) [*Bader et al*., 2012b]. We place another subduction zone south of the Songshugou complex and equivalent ultramafic rocks in the northernmost Danfeng complex (Figure 14a). This N-dipping subduction caused exhumation of a hanging-wall mantle sliver, the Songshugou ultramafic rocks, and the emplacement of the Fushui intrusives, potentially an ultramafic-mafic arc complex; the mantle sliver preserved Late Cambrian (U)HT metamorphism (mafic HP granulites). This granulite-facies metamorphism in the Songshugou complex (830–920°C, 1.0–1.6 GPa) at ~501 Ma needed high heat flow; the crustal base of an active arc, the Fushui complex, provided an appropriate setting for a metamorphic overprint at such high temperatures, i.e., a high heat flow together with magmatic underplating. During further subduction-accretion of buoyant lithosphere (see below), the mafic and ultramafic rocks were exhumed. This subduction zone and possibly the one to the north imprinted the pre-~460 Ma magmatism and associated HT metamorphism across the Qinling complex. The oldest, well-documented metamorphic age in the Qinling complex is the ~520 Ma monazite age from the western central Qinling garnet-sillimanite gneisses (Guokou "Formation") [*Chen et al*., 2006]. *Dong et al*.'*s* [2011c] low Th/U ~514 Ma zircons from migmatitic gneiss likely record the earliest migmatization event. These are followed by metamorphic zircon and monazite ages to ~459 Ma (Figures 5a, 5l, and 11c). Continuous magmatism started at ~515 Ma with possible precursors as early as ~586 Ma (Figures 5l, 11b, and 11d).

[52] Possibly intraoceanic subduction caused the establishment of a relatively short-lived oceanic basin, the Danfeng complex (~50 Myr, 520–470 Ma; metabasite dominated part, Figures 6a and 14a) within the wide oceanic domain between the Qinling complex and the SCC. Entrance of this relative young lithosphere into the N-dipping subduction underneath the Songshugou-Fushui-Qinling complexes may have caused shortening across these northern complexes that may have supported the exhumation of the (U)HP rocks to the north; the buoyant lithosphere may also have decreased igneous activity at ~460 Ma. Subsequent subduction of the Danfeng spreading ridge (Figure 14b) caused flare-up of magmatism, peaking at ~430 Ma in the Qinling complex, and regional HT/UM metamorphism, peaking at 420–400 Ma; this scenario is consistent with the interpretation of UHT/UM metamorphism in the Tongbai Shan [*Xiang et al*., 2012]. Subduction continued south of the Danfeng-complex lithosphere, leaving remnant oceanic lithosphere, the Danfeng complex, as the base of a fore-arc basin, the Liuling complex (Figure 14b) [e.g., *Ratschbacher et al*., 2003, 2006]. This N-dipping subduction continued until the terminal NCC-SCC collision, with the subduction of the northern margin of SCC, the Yangtze block, to mantle depth in the Triassic. Subduction of old oceanic lithosphere led to diminishing magmatic activity; it imprinted, however, a distinct Late Devonian–Permian metamorphic record onto the fore-arc basin, the southward adjoining accretionary wedge, and footwall Yangtze craton (see detailed evaluation in part III of this series of papers); this is the Late Devonian–Carboniferous "reheating event" in the Qinling and Erlangping complexes. The Erlangping complex may have been inverted from spreading to subduction at the time of subduction of the buoyant Danfeng-complex oceanic lithosphere (Figure 14b). We note that the suggested time of subduction of buoyant lithosphere and spreading-ridge subduction (starting at ~460 Ma) is also the time of the Kawansian intraplate orogen (~460–440 Ma peak magmatism and metamorphism) between the Yangtze and Cathaysia blocks that cratonized the SCC (Figures S1 and 14b); it is also the time of major subsidence of and the emplacement of sills and a dike swarm into the Yangtze passive margin (~440 Ma; Figure 14b).

[53] Although a detailed assessment is beyond the scope of this paper, we note that our scenario correlates well with the scenario of magmatism and (U)HP and HT metamorphism in the Qaidam basin–Qilian block orogenic collage >500 km to the west (Figures 1 and 14c) [e.g., *Tseng et al*., 2009; *Mattinson et al*., 2009; *Xiong et al*., 2011; *Tung et al*., 2012; *Zhang et al*., 2012, and references therein]. There, the Tarim block replaces the NCC and the North-Qilian island arc is equivalent to the Erlangping complex. The Qilian block has a similar Meso-Neoproterozoic core than the Qinling complex, and the North-Qilian HP-UHP subduction-accretion wedge corresponds to the North-Qinling complex. In the south, the S-Qilian subduction-accretion wedge is equal to the eclogite and gneiss-amphibolite-migmatite association of the central and southern Qinling complex, and the Shenglikou (Lüliangshan) UHP peridotite massif corresponds in tectonic position to the Songshugou complex; both complexes are overprinted by an arc (Fushui intrusions in the Qinling). The entire Qilian block features a massive Early Paleozoic arc (Qilian arc), like the Qinling complex. Finally, an even more southerly, N-dipping subduction zone existed, imprinting the Late Paleozoic–Early Mesozoic Kunlun arc onto the southern margin of the Qaidam block. The latter pinches out eastward, but the Kunlun suture (also Amnyemaqen-Kunlun-Mutztagh suture) can be connected with the subduction zone south of the Liuling fore-arc basin; the Danfeng complex thus replaces the Qaidam block. This is not exceptional: the Danfeng complex also pinched out eastward, and thus, no Silurian-Devonian magmatism and HT metamorphism occurred in the Qinling complex of the northern Dabie Shan and Sulu region east of

the Tongbai Shan. Finally, also the Qinling complex disappears eastward, being absent in the Sulu.

5. Conclusions

[54] Enough is now known about the Early Paleozoic evolution of the Qinling orogenic collage to present a reinterpretation of its tectonic history (Figure 14). The principal results are as follows:

[55] 1. The Qinling-Tongbai orogen contains snapshots of (U)HP and (U)HT metamorphic evolutions. The North-Qinling complex comprises a P-T path from ~550°C, 3.1 GPa in the diamond-coesite stability field to quartz-eclogite facies recrystallization at ~660°C, 2.0–2.3 GPa, and nearly isothermal decompression, to 630–640°C, 1.1–1.5 GPa. Published U-Pb geochronology using zircons with diamond inclusions and new U-Pb titanite and ^{40}Ar-^{39}Ar phengite ages constrain this path from UHP metamorphism to cooling below ~400°C in the crust between ~500 and ~470 Ma. South of the Meso-Neoproterozoic core of the Qinling complex, published eclogite data yielded 630–720°C, 2.5–3.0 GPa and 696 ± 56°C, 1.4 ± 0.3 GPa for peak and retrograde conditions; peak condition are dated at ~490–473 Ma, retrograde at ~400 Ma. Garnet amphibolite adjacent to the Songshugou ultramafic complex south of the Qinling complex recorded a prograde P-T path, ~498°C, 2.25 GPa to ~530°C, 2.54 GPa; its age is older than ~425 Ma. Published data show that mafic granulites of the Songshugou complex evolved from a possible early HT eclogite stage to peak-T metamorphism at 830–920°C, 1.0–1.6 GPa to ≤700°C, 0.6–0.9 GPa; peak metamorphism occurred at ~500 Ma. The entire Qinling complex and most of the Songshugou-Fushui complex underwent an upper amphibolite facies, UM overprint at 680–775°C and 0.5–0.75 GPa at ~425–395 Ma; published estimates in the Tongbai Shan for the same event peak at 880–920°C, 0.8–1.0 GPa, with relics of UHT metamorphism at >940°C.

[56] 2. Tectonostratigraphic, metamorphic, and geochronologic data derived from the various complexes in the Qinling orogenic collage are the base for a new tectonic model that integrates these (U)HP and (U)HT evolutions and the oceanic domains that surrounded the Meso-Neoproterozoic core of the Qinling complex. After post-supercontinent Rodinia rifting and oceanic spreading had established wide ocean basins, intraoceanic subduction formed the UHP North-Qinling complex subduction-accretion wedge north of Meso-Neoproterozoic core of the Qinling complex; the Erlangping complex constituted an intraoceanic arc–back-arc system to this subduction. Another subduction-accretion system nucleated south of the Qinling-complex core; it formed the Qinling-complex eclogite and the Songshugou HP garnet amphibolite. A further subduction-accretion system south of the Songshugou complex caused exhumation of a hanging-wall mantle sliver, the Songshugou ultramafic rocks, and the emplacement of the Fushui intrusives, potentially ultramafic-mafic arc rocks. This subduction zone and possibly the one to the north imprinted the pre-~460 Ma magmatism and the associated first period (>460 Ma) of HT metamorphism across the Qinling complex.

[57] Intraoceanic subduction caused the establishment of a relatively short-lived oceanic basin, the Danfeng complex (~50 Myr, 520–470 Ma) within the wide oceanic domain between the Qinling complex and the SCC. Entrance of this relatively young lithosphere and subsequent subduction of the Danfeng spreading ridge caused flare-up of magmatism, peaking at ~430 Ma in the Qinling complex, and regional (U)HT-UM at ~420–400 Ma. Subduction continued south of the Danfeng-complex lithosphere, leaving remnant oceanic lithosphere, the Danfeng complex, as the base of a fore-arc basin. This N-dipping subduction continued until the terminal NCC-SCC collision in the Triassic. This scenario is compatible with the Qaidam-Qilian subduction-accretion system, the western branch of the "Heart of China" orogen.

Appendix A: Compilation, Recalculation, and Presentation of Published Data

[58] The U/Th-Pb geochronology summarized in Table S1 was derived from the original data tables. We recalculated several samples important to our analysis; this was done in particular for Chinese language papers, in cases of incomplete presentation (e.g., emphasis on a specific age group), or when we chose to highlight particular aspects of the data (e.g., the Paleozoic age clusters in a detrital zircon sample) that were not the focus of the original publication; these specific cases are discussed in the course of the paper. In our recalculations, we used concordant data (±10%) and prioritized ^{238}U/^{206}Pb-^{207}Pb/^{206}Pb concordia ages over ^{238}U/^{206}Pb or ^{207}Pb/^{206}Pb weighted mean ages (for definitions, see *Ludwig* [2008]) that are widespread in the literature; these dates commonly include discordant zircons in the mean age calculation.

[59] Where available, Table S1 provides data important for the scope of this paper, e.g., the number of data used in the age calculation, upper or lower intercept ages, Th/U ratios, magmatic versus metamorphic zircon interpretation, cathodoluminescence (CL) appearance, and interpretations favored by the authors. To allow identification, we provide, where given, original sample number, rock type, geologic unit, and location description.

[60] In the data presentation, we made use of tools provided within Isoplot [*Ludwig*, 2008] and by the University of Arizona laser-chronology laboratory [https://sites.google.com/a/laserchron.org/laserchron/home/]. For regional age comparisons, e.g., among the various complexes of the Qinling-Tongbai orogenic collage, we use cumulative age probability plots that are normalized by the number of analyses. When reporting the duration of apparently continuous magmatic-metamorphic events/cycles, we display (in the Figures) and report (in the text) the range of the relevant age populations. We used several ways to analyze specific events/cycles represented by the geochronologic data: (i) we employed linearized probability plots to evaluate whether or not a suite of data conforms to a normal distribution (represented by a linear distribution with a slope of 1; not shown in the paper), and (ii) we highlighted the specific events/cycles by both "robust means" (i.e., Tukey's biweight means [*Hoaglin et al*., 1983] best-suited to a normal data distribution, contaminated by data not belonging to that distribution; see *Ludwig* [2008]), and medians. Such means/medians are thought as aiding the comparison of events and approximate the peak activities (magmatism or metamorphism).

[61] **Acknowledgments.** The study was supported by Swiss National Science Foundation grants 200021-113300/1 and 200020-129907/1 to LF and DFG (RA442/25) and Robert Bosch Foundation grants to LR. We thank Oona Appelt, Dieter Rhede (GFZ Potsdam), and Axel Renno (Freiberg) for help with the microprobe. Bradley R. Hacker (UCSB) supported this study by zircon and titanite analyses of several samples at the University of Arizona, Tucson, and University of California, Santa Barbara, discussion, and by polishing our paper's language. EMP profiles were plotted using GMT (Paul Wessel and Walter H. F. Smith, http://www.soest.hawaii.edu/gmt/). Eva Enkelmann and Maria Wiesinger shared parts of the fieldwork; George Gehrels provided access to University of Arizona's laserchron laboratory, and Axel Schmitt to UCLA's SIMS facility. Yunpeng Dong (Xi'an) is thanked for a visit to Freiberg; the controversial but enlightening discussion with him prompted LR to compile this paper. John Wakabayashi, Uwe Altenberger, and two anonymous reviewers are thanked for detailed and helpful reviews.

References

Bader, T., L. Franz, C. de Capitani, J. Mullis, and L. Zhang (2012a), The granulite-facies metamorphism in the Tongbai area (east-central China): New insights from spinel-bearing equilibrium-assemblage calculations, and fluid inclusions, *Geophys. Res. Abstr.*, *14*, EGU 2012–3912.

Bader, T., L. Zhang, L. Franz, L. Ratschbacher, and C. de Capitani (2012b), The enigmatic Songshugou complex (Qinling orogen, central China): Mélange of high-pressure and (ultra)high-temperature metamorphic rocks?, Abstract 10th Swiss Geoscience Meeting, Bern 2012.

Bader, B., L. Ratschbacher, L. Franz, Z. Yang, M. Hofmann, U. Linnemann, and H. Yang (2013), The Heart of China revisited, I. Proterozoic tectonics of the Qin Mountains in the core of supercontinent Rodinia, *Tectonics*, *32*, 1–27, doi:10.1002/tect.20024.

Ballhaus, C., R. F. Berry, and D. H. Green (1991), High-pressure experimental calibration of the olivine-orthopyroxene-spinel oxygen geobarometer: Implications for the oxidation state of the upper mantle, *Contrib. Min. Pet.*, *107*, 27–40.

Bhadra, S., and A. Bhattacharya (2007), The barometer tremolite + tschermakite + 2 albite = 2 pargasite + 8 quartz: Constraints from experimental data at unit silica activity, with application to garnet-free natural assemblages, *Am. Mineral.*, *92*, 491–502, doi:10.2138/am2007.2067.

Chen, D., L. Liu, Y. Sun, A. Zhang, X. Liu, and J. Luo (2004), LA-ICP-MS zircon U-Pb dating for high-pressure basic granulite from North Qinling and its geological significance, *Chin. Sci. Bull.*, *49*, 2296–2304.

Chen, Q., N. Chen, Q. Wang, M. Sun, X. Wang, X. Li, and S. Shu (2006), Electron microprobe chemical ages of monazite from Qinling Group in the Qinling Orogen: Evidence for Late Pan-African metamorphism?, *Chin. Sci. Bull.*, *51*, 2645–2650.

Cheng, H., C. Zhang, J. D. Vervoort, X. Li, Q. Li, S. Zheng, and D. Cao (2011), Geochronology of the transition of eclogite to amphibolite facies metamorphism in the North Qinling orogen of central China, *Lithos*, *125*, 969–983, doi:10.1016/j.lithos.2011.05.010.

Cheng, H., C. Zhang, J. D. Vervoort, X. Li, Q. Li, Y. Wu, and S. Zheng (2012), Timing of eclogite facies metamorphism in the North Qinling by U–Pb and Lu–Hf geochronology, *Lithos*, *136–139*, 46–59, doi:10.1016/j.lithos.2011.06.003.

Colombi, A. (1988), Métamorphisme et géochimie des roches mafiques des Alpes ouest-centrales (géopofil Viège Domodossola-Locarno), PhD thesis, University Lausanne, Switzerland, 216 p.

Diwu, C. R., Y. Sun, L. Liu, C. L. Zhang, and H. L. Wang (2010), The disintegration of Kuanping Group in North Qinling orogenic belt and Neo-Proterozoic N-MORB basalt, *Acta Petrol. Sinica*, *26*, 2025–2038.

Dong, Y., D. Zhou, and G. Zhang (1997a), Geochemistry and formation setting of Fushui complex, eastern Qinling, *Geochimica*, *26*, 79–88.

Dong, Y., D. Zhou, and L. Liu (1997b), Sm-Nd isotopic ages of the Songshugou ophiolite from the east Qinling and its geological significance, *Regional Geol. Chin.*, *16*, 217–221.

Dong, Y., M. Zhou, G. Zhang, D. Zhou, L. Liu, and Q. Zhang (2008), The Grenvillian Songshugou ophiolite in the Qinling Mountains, Central China: Implications for the tectonic evolution of the Qinling orogenic belt, *J. Asian Earth Sci.*, *32*, 325–335, doi:10.1016/j.jseaes.2007.11.010.

Dong, Y., G. Zhang, F. Neubauer, X. Liu, J. Genser, and C. Hauzenberger (2011a), Tectonic evolution of the Qinling orogen, China: Review and synthesis, *J. Asian Earth Sci.*, *41*, 213–237, doi:10.1016/j.jseaes.2011.03.002.

Dong, Y., G. Zhang, C. Hauzenberger, F. Neubauer, Z. Yang, and X. Liu (2011b), Paleozoic tectonics and evolutionary history of the Qinling orogen: Evidence from geochemistry and geochronology of ophiolite and related volcanic rocks, *Lithos*, *122*, 39–56, doi:10.1016/j.lithos.2010.11.011.

Dong, Y., J. Genser, F. Neubauer, G. Zhang, X. Liu, Z. Yang, and B. Heberer (2011c), U-Pb and $^{40}Ar/^{39}Ar$ geochronological constraints on the exhumation history of the North Qinling terrane China, *Gondwana Res.*, *19*, 881–893, doi:10.1016/j.gr.2010.09.007.

Gao, S., J. Yang, L. Zhou, M. Li, Z. Hu, J. Guo, H. Yuan, H. Gong, G. Xiao, and J. Wei (2011), Age and growth of the Archean Kongling terrain, South China, with emphasis on 3.3 Ga granitoid gneisses, *Am. J. Sci.*, *311*, 153–182, doi:10.2475/02.2011.03.

Glazner, A. F., J. M. Bartley, D. S. Coleman, W. Gray, and R. Z. Taylor (2004), Are plutons assembled over millions of years by amalgamation from small magma chambers?, *GSA Today*, *14*, 4–11, doi:10.1130/1052-5173(2004)014<0004:APAOMO>2.0.CO;2.

Hacker, B. R., L. Ratschbacher, and J. G. Liou (2004), Subduction, collision and exhumation in the ultrahigh-pressure Qinling-Dabie orogen, in *Aspects of the Tectonic Evolution of China*, vol. 226, edited by J. Malpas et al, pp. 157–175, Geol. Soc. London, Spec. Publ.

He, Y. H., G. C. Zhao, M. Sun, and X. P. Xia (2009), SHRIMP and LA-ICP-MS zircon geochronology of the Xiong'er volcanic rocks: Implications for the Paleo-Mesoproterozoic evolution of the southern margin of the North China Craton, *Precambrian Res.*, *168*, 213–222, doi:10.1016/j.precamres.2008.09.011.

Hoaglin, D. C., F. Mosteller, and J. W. Tukey (1983), *Understanding Robust and Exploratory Data Analysis*, pp. 345–349, John Wiley and Sons, New York.

Hu, N. G., D. G. Zhao, B. Q. Xu, and T. Wang (1995a), Discovery of coesite-bearing eclogites from the Northern Qinling and its significances, *Chin. Sci. Bull.*, *40*, 174–176.

Hu, N. G., D. G. Zhao, B. Q. Xu, and T. Wang (1995b), Petrography and metamorphism study on high-ultrahigh pressure eclogite from Guanpo area, northern Qinling Mountains, *J. Mineral. Petrol.*, *15*, 1–9.

Kretz, R. (1983), Symbols for rock-forming minerals, *Am. Mineral.*, *68*, 277–279.

Krogh Ravna, E., and M. P. Terry (2004), Geothermobarometry of UHP and HP eclogites and schists—An evaluation of equilibria among garnet-clinopyroxene-kyanite-phengite-coesite/quartz, *J. Metamorph. Geol.*, *22*, 579–592, doi:10.1111/j.525-1314.2004.00534.x.

Leake, B. E., et al. (1997), Nomenclature of amphiboles: Report of the subcommittee on amphiboles of the International Mineralogical Association, commission on new minerals and mineral names, *Can. Mineral.*, *35*, 219–246.

Li, S., Y. Chen, G. Zhang, and Z. Zhang (1991), A 1 Ga Alpine peridotite body emplaced into the Qinling Group: Evidence for the existence of the late Proterozoic plate tectonics in the North Qinling area, *Geol. Rev.*, *37*, 235–242.

Li, W., T. Wang, X. Wang, and H. Cao (2000), Single zircon dating of the Huichizi complex, north Qinling: Its geological significance, *Regional Geol. Chin.*, *19*, 172–174.

Li, Z. X., et al. (2008a), Assembly, configuration, and break-up history of Rodinia: A synthesis, *Precambrian Res.*, *160*, 179–210, doi:10.1016/j.precamres.2007.04.021.

Li, W., X. Li, and Z. Li (2008b), Middle Neoproterozoic syn-rifting volcanic rocks in Guangfeng, South China: Petrogenesis and tectonic significance, *Geol. Mag.*, *145*, 475–489, doi:10.1017/S0016756808004561.

Liu, J., and Y. Sun (2005), New data on the "hot" emplacement age of ultramafic rocks from the Songshugou area in the Eastern Qinling, *Geol. Rev.*, *51*, 198–192.

Liu, L., D. Zhou, Y. Dong, H. Zhang, Y. Liu, and Z. Zhang (1995), High pressure metabasites and their retrograde metamorphic P-T-t path from Songshugou area, eastern Qinling Mountains, *Acta Petrol. Sinica*, *11*, 127–136.

Liu, L., D. Zhou, Y. Wang, D. Chen, and Y. Liu (1996), Study and implication of the high-pressure felsic granulite in the Qinling complex of East Qinling, *Sci. China, Ser. D*, *39*, Supplement, 60–68.

Liu, L., D. Chen, A. Zhang, C. Zhang, H. Yuna, and J. Luo (2004), Geochemical characteristics and LA-ICPM-MS zircon U-Pb dating of amphibolites in the Songshugou ophiolite in the eastern Qinling, *Acta Geol. Sinica*, *78*, 137–145.

Liu, J., Y. Sun, T. Lai, and W. Sun (2009), Emplacement age of the Songshugou ultramafic massif in the Qinling orogenic belt, and geologic implications, *Int. Geol. Rev.*, *51*, 58–76, doi:10.1080/00206810802650576.

Liu, X., B.-M. Jahn, J. Hua, S. Li, X. Liu, and B. Song (2011), Metamorphic patterns and SHRIMP zircon ages of medium- to high-grade rocks from the Tongbai orogen, central China: Implications for multiple accretion/collision processes prior to terminal continental collision, *J. metamorph. Geol.*, *29*, 979–1002, doi:10.1111/j.1525-1314.2011.00952.x.

Ludwig, K. R. (2008), Isoplot 3.70. A geochronological toolkit for Microsoft Excel, *Berkeley Geochronol. Center Spec. Publ.*, *4*, 1–76.

Mattinson, C. G., J. L. Wooden, J. X. Zhang, and D. K. Bird (2009), Paragneiss zircon geochronology and trace element geochemistry, North

Qaidam HP/UHP terrane, western China, *J. Asian Earth Sci.*, *35*, 298–309, doi:10.1016/j.jseaes.2008.12.007.

Mehnert, K. R. (1968), *Migmatites and the Origin of Granitic Rocks, Developments in Petrology, 1*, pp. 393, Elsevier Publishing Company, Amsterdam – London – New York.

Meng, Q., and G. Zhang (2000), Geologic framework and tectonic evolution of the Qinling orogen, central China, *Tectonophysics*, *323*, 183–196.

O'Neill, H. S. C., and V. J. Wall (1987), The olivine-spinel oxygen geobarometer, the nickel precipitation curve, and the oxygen fugacity of the Earth's upper mantle, *J. Petrol.*, *6*, 1169–1191.

Okay, A. I., A. M. C. Sengör, and M. Satir (1993), Tectonics of an ultrahigh-pressure metamorphic terrane: Dabie Shan, China, *Tectonics*, *12*, 1320–1334.

Peng, S., T. M. Kusky, X. F. Jiang, L. Wang, J. P. Wang, and H. Deng (2012), Geology, geochemistry, and geochronology of the Miaowan ophiolite, Yangtze craton: Implications for South China's amalgamation history with the Rodinian supercontinent, *Gondwana Res.*, *21*, 577–594, doi:10.1016/j.gr.2011.07.010.

Ratschbacher, L., B. R. Hacker, A. Calvert, A. L. E. Webb, J. C. Grimmer, M. McWilliams, T. Ireland, S. Dong, and J. Hu (2003), Tectonics of the Qinling Belt (Central China): Tectonostratigraphy, geochronology, and deformation history, *Tectonophysics*, *366*, 1–53, doi:10.1016/S0040-1951(03)00053-2.

Ratschbacher, L., L. Franz, E. Enkelmann, R. Jonckheere, A. Pörschke, B. R. Hacker, S. Dong, and Y. Zhang (2006), The Sino-Korean–Yangtze suture, the Huwan detachment, and the Paleozoic–Tertiary exhumation of (ultra)high-pressure rocks along the Tongbai–Xinxian–Dabie Mountains, in *Ultrahigh-Pressure Metamorphism: Deep Continental Subduction*, *403*, edited by B. R. Hacker, W. C. McClelland, and J. G. Liu, pp. 44–75, Geological Society of America Special Paper, Boulder, doi:10.1130/2006.2403(03).

Shi, Y., J. H. Yu, X. S. Xu, J. S. Qiu, and L. H. Chen (2009), Geochronology and geochemistry of the Qinling Group in the eastern Qinling orogen, *Acta Petrol. Sinica*, *25*, 2651–2670.

Spear, F. S. (1993), *Metamorphic Phase Equilibria and Pressure Temperature Time Paths*, pp. 799, Mineralogical Society of America, Washington, D.C.

Su, L., S. Song, B. Song, D. Zhou, and J. Hao (2004), SHRIMP zircon U-Pb ages of garnet pyroxenite and Fushui gabbroic complex in Songshugou region and constraints on tectonic evolution of Qinling Orogenic Belt, *Chin. Sci. Bull.*, *49*, 1307–1310.

Sun, W., I. S. Williams, and S. Li (2002), Carboniferous and Triassic eclogites in the western Dabie Mountains, east-central China: Evidence for protracted convergence of the North and South China Blocks, *J. Metamorph. Geol.*, *20*, 873–886.

Tseng, C., H. Yang, H. Yang, D. Liu, C. Wu, C. Cheng, C. Chen, and C. Ker (2009), Continuity of the North Qilian and North Qinling orogenic belts, Central Orogenic System of China: Evidence from newly discovered Paleozoic adakitic rocks, *Gondwana Res.*, *16*, 285–293, doi:10.1016/j.gr.2009.04.003.

Tung, K., H. Yang, D. Liu, J. Zhang, H. Yang, Y. Shau, and C. Tseng (2012), The amphibolite-facies metamorphosed mafic rocks from the Maxianshan area, Qilian block, NW China: A record of early Neoproterozoic arc magmatism, *J. Asian Earth Sci.*, *46*, 177–189, doi:10.1016/j.jseaes.2011.12.006.

Vermeesch, P. (2012), On the visualisation of detrital age distributions, *Chem. Geol.*, *312–313*, 190–194, doi:10.1016/j.chemgeo.2012.04.021.

Wang, T., X. Wang, G. Zhang, X. Pei, and C. Zhang (2003), Remnants of a Neoproterozoic collisional orogenic belt in the core of the Phanerozoic Qinling orogenic belt (China), *Gondwana Res.*, *6*, 699–710.

Wang, T., X. Wang, W. Tian, C. Zhang, W. Li, and S. Li (2009), North Qinling Paleozoic granite associations and their variation in space and time: Implications for orogenic processes in the orogens of central China, *Sci. China, Ser. D*, *52*, 1359–1384.

Wang, H., Y.-B. Wu, S. Gao, X.-C. Liu, H.-J. Gong, Q.-L. Li, X.-H. Li, and H.-L. Yuan (2011a), Eclogite origin and timing in the North Qinling terrane, and their bearing on the amalgamation of the South and North China blocks, *J. metamorph. Geol.*, *29*, 1019–1031, doi:10.1111/j.1525-1314.2011.00955.x.

Wang, Y., A. Zhang, W. Fan, G. Zhao, G. Zhang, Y. Zhang, F. Zhang, and S. Li (2011b), Kwangsian crustal anatexis within the eastern South China Block: Geochemical, zircon U–Pb geochronological and Hf isotopic fingerprints from the gneissoid granites of Wugong and Wuyi–Yunkai domains, *Lithos*, *127*, 239–260, doi:10.1016/j.lithos.2011.07.027.

Wu, Y., Y. Zheng, S. Gao, W. Jiao, and Y. Liu (2008), Zircon U–Pb age and trace element evidence for Paleoproterozoic granulite-facies metamorphism and Archean crustal rocks in the Dabie Orogen, *Lithos*, *101*, 308–322, doi:10.1016/j.lithos.2007.07.008.

Xiang, H., L. Zhang, Z. Zhong, M. Santosh, H. Zhou, H. Zhang, J. Zheng, and S. Zheng (2012), Ultrahigh-temperature metamorphism and anticlockwise P-T-t path of Paleozoic granulites from north Qinling-Tongbai orogen, Central China, *Gondwana Res.*, *21*, 559–576, doi:10.1016/j.gr.2011.07.002.

Xiong, Q., J. Zheng, W. L. Griffin, S. Y. O'Reilly, and J. Zhao (2011), Zircons in the Shenglikou ultrahigh-pressure garnet peridotite massif and its country rocks from the North Qaidam terrane (western China): Meso-Neoproterozoic crust–mantle coupling and early Paleozoic convergent plate-margin processes, *Precambrian Res.*, *187*, 33–57, doi:10.1016/j.precamres.2011.02.003.

Xu, C., I. H. Campbell, C. M. Allen, Y. Chen, Z. Huang, L. Qi, G. Zhang, and Z. Yan (2008), U–Pb zircon age, geochemical and isotopic characteristics of carbonatite and syenite complexes from the Shaxiongdong China, *Lithos*, *105*, 118–128, doi:10.1016/j.lithos.2008.03.002.

Xue, F., A. Kröner, T. Reischmann, and F. Lerch (1996), Paleozoic pre- and post-collision calc-alkaline magmatism in the Qinling orogenic belt, central China, as documented by zircon ages on granitoid rocks, *J. Geol. Soc. London*, *153*, 409–417.

Yan, Q., J. Chen, Z. Wang, Z. Yan, T. Wang, Q. Li, Z. Zhang, and C. Jiang (2008), Zircon U-Pb and geochemical analyses for leucocratic intrusive rocks in pillow lavas in the Danfeng Group, north Qinling Mountains China, *Sci. China, Ser. D*, *51*, 249–262.

Yang, J., et al. (2003), Discovery of metamorphic diamonds in central China: An indication of a > 4000-km-long zone of deep subduction resulting from multiple continental collisions, *Terra Nova*, *15*, 370–379, doi:10.1046/j.1365-3121.2003.00511.x.

Yang, J., F. Liu, C. Wu, Z. Xu, R. Shi, S. Chen, E. Deloule, and J. L. Wooden (2005), Two ultrahigh-pressure metamorphic events recognized in the central orogenic belt of China: Evidence from the U-Pb dating of coesite-bearing zircons, *Int. Geol. Rev.*, *47*, 327–343.

You, Z., Y. Han, S. Suo, N. Chen, and Z. Zhong (1993), Metamorphic history and tectonic evolution of the Qinling Complex, eastern Qinling Mountains, China, *J. Metamorph. Geol.*, *11*, 549–560.

Zhang, E. (1992), *Geological Map of Qinling-Daba Mountains and Adjacent Areas, 1:1.000.000*, Geological Publishing House, Beijing.

Zhang, Z. (1999), Metamorphic evolution of garnet-clinopyroxene-amphibole rocks from the Proterozoic Songshugou mafic-ultramafic complex, Qinling Mountains, central China, *Island Arc*, *8*, 259–280.

Zhang, G., B. Zhang, X. Yuan, and Q. Xiao (2001), *Qinling Orogenic Belt and Continental Dynamics*, pp. 855, Science Press, Beijing.

Zhang, C., H. van Roermund, L. Zhang, and C. Spiers (2012), A polyphase metamorphic evolution for the Xitieshan paragneiss of the north Qaidam UHP metamorphic belt, western China: In-situ EMP monazite- and U–Pb zircon SHRIMP dating, *Lithos*, *136–139*, 27–45, doi:10.1016/j.lithos.2011.07.024.

Zhu, X., F. Chen, S. Li, Y. Yang, H. Nie, W. Siebel, and M. Zhai (2011), Crustal evolution of the North Qinling terrain of the Qinling Orogen, China: Evidence from detrital zircon U–Pb ages and Hf isotopic composition, *Gondwana Res.*, *20*, 194–204, doi:10.1016/j.gr.2010.12.009.